IL-27 limits HSPC differentiation during infection and protects from stem cell exhaustion

Daniel L. Aldridge[1], Zachary Lanzar[1], Anthony T. Phan[1], David A. Christian[1], Ryan Pardy[1], Booki Min[2], Ross M. Kedl[3], Christopher A. Hunter[1]

[1]University of Pennsylvania School of Veterinary Medicine, Philadelphia, PA, USA

[2]Department of Microbiology and Immunology, Feinber School of Medicine, Northwestern University, Chicago, IL, USA

[3]University of Colorado, Anschuitz Medical Campus, Aurora, CO, USA

Abstract

Many inflammatory stimuli can induce progenitor cells in the bone marrow to produce increased numbers of myeloid cells as part of the process of emergency myelopoiesis. These events are associated with trained immunity and have long-term impacts on hematopoietic stem and progenitor cell (HSPC) development but can also compromise their function. While many cytokines support emergency myelopoiesis, less is known about the mechanisms that temper these events. When mice that lack the cytokine IL-27 were infected with *Toxoplasma gondii*, there was enhanced generation of monocyte progenitors and increased numbers of inflammatory monocytes. In the bone marrow of infected mice there was increased production of IL-27 that localized with HSPCs and a survey of cytokine receptor expression highlighted that HSPCs were uniquely poised to respond to IL-27. Furthermore, the use of *in vitro* differentiation assays and mixed bone marrow chimeras revealed that HSPCs from IL-27 deficient mice are pre-disposed towards the monocyte lineage. Additional studies highlighted that after infection loss of the IL-27R resulted in reduced HSPC fitness that manifested as reduced proliferative responses and a decreased ability to reconstitute the hematopoietic system. Thus, the ability of IL-27 to act on HSPC provides a regulatory brake on differentiation to limit monocyte induction and preserve HSPC stemness.

Introduction

In response to inflammatory stimuli, cytokine production can directly affect progenitor populations in the bone marrow leading to alterations in hematopoiesis (Collins et al., 2021). For example, in response to microbial challenges, elevated levels of GM-CSF, IFN-γ, and IL-6 modulate hematopoietic stem and progenitor cell (HSPC), which contain hematopoietic stem cells (HSCs) as well as multipotent progenitors (MPP), differentiation and enhance myelopoiesis (Baldridge et al., 2010; Kaufmann et al., 2018; Khan et al., 2020; Link, 2000; MacNamara et al., 2011a; MacNamara et al., 2011b; Maeda et al., 2005; Matatall et al., 2014; Miner et al., 2021; Mirantes et al., 2014; Reynaud et al., 2011). These events can also lead to long-term epigenetic and metabolic changes in HSCs that forms the basis for the process of trained immunity (Ochando et al., 2023). Thus, many of the cytokines produced during different infections are associated with trained immunity (Kaufmann et al., 2018; Khan et al., 2020). For example, after challenge with *Mycobacterium avium* or SARS-COV-2, IFN-γ and IL-6, respectively, can skew HSCs towards myeloid output and increase the functionality of their downstream progeny (Cheong et al., 2023; Matatall et al., 2014).

While trained immunity is associated with long-term changes to hematopoietic stem cells (HSC), inflammation can also reduce HSC functionality, which can manifest as decreased proliferative and differentiation potential. To mitigate these adverse effects, there are cell-intrinsic mechanisms such as autophagic processes to limit oxidative damage, epigenetic reprogramming, and metabolic changes that contribute to the maintenance of stemness (Ibneeva et al., 2024; Liu et al., 2020; Ma et al., 2020; Revuelta and Matheu, 2017; Singh et al., 2018; Zhao and Deininger, 2023). Without these protective mechanisms, HSCs accumulate cellular damage and lose their ability to self-renew and differentiate, a process termed stem cell exhaustion. While inflammation

56 is linked to HSC exhaustion, less is known about the cell extrinsic factors that contribute to the
57 maintenance of HSC quiescence and integrity, but several cytokines have been implicated in this
58 process. For example, in response to repeated stimulation with poly I:C, IFN-α can remove actively
59 proliferating HSCs from the developmental pool as a mechanism to prevent the accumulation of
60 damaged HSCs (Pietras et al., 2014). In addition, during fetal development there is evidence that
61 IL-10 limits HSC responsiveness to inflammatory signaling and thereby limit emergency
62 myelopoiesis as a mechanism to preserve HSC functionality (Collins et al., 2024).

63 IL-27 is a member of the Type I family of cytokines that utilize JAK-STAT signaling to
64 mediate their biological effects. This family also includes IL-6, and both of these cytokines signal
65 through dimeric receptors that contain the gp130 receptor combined with unique IL-6Rα and IL-
66 27Rα components. Because T cells constitutively express high levels of the IL-27R (Pflanz et al.,
67 2004; Pflanz et al., 2002), the majority of studies on this cytokine have focused on its impact on
68 these populations. Thus, IL-27 can limit the development of pathological Th1, Th2, and Th17
69 $CD4^+$ T cell responses (Findlay et al., 2010; Hamano et al., 2003; Villarino et al., 2003), but several
70 studies have also indicated that the absence IL-27 results in an elevated population of inflammatory
71 monocytes that contribute to the development of immune pathology (Aldridge et al., 2024; Liu et
72 al., 2021). The observation that the loss of IL-27 also results in enhanced inflammatory monocyte
73 induction prior to a detectable T cell response suggests that IL-27 may antagonize the innate
74 events that promote these monocyte populations (Aldridge et al., 2024). Consistent with this
75 idea, there are additional reports that IL-27 can limit neutrophil and monocyte responses
76 and directly impact myelopoiesis (Furusawa et al., 2016; Liu et al., 2014; Liu et al., 2021; Seita
77 et al., 2008; Sun et al., 2017; Wirtz et al., 2006). However, the observation that monocytes do not
78 express the IL-27R suggests that the ability of IL-27 to modulate this population is indirect.

79 The studies presented here show that infection with *T. gondii* results in increased activity
80 of HPSC and downstream progenitors associated with emergency myelopoiesis; however, in the
81 absence of IL-27, HSPCs display a skewed developmental program that resulted in enhanced
82 monopoiesis. While all HSPCs showed preferential expression of the IL-27R, with LTHSCs and
83 MPP2s exhibiting the highest, the loss of IL-27 during infection resulted in reduced HSPC fitness.
84 Thus, during infection, the ability of IL-27 to act on HSPC provides a regulatory brake on
85 differentiation to limit monocyte induction and preserve HSPC stemness.
86

87 **Materials and Methods**

88 **Mice and infection**

89 Female and male C57BL/6 mice were purchased (8-12 weeks old; strain # 000664) from
90 Jackson labs as age and sex matched controls for whole body knockout mice. CD45.1 donor mice
91 were either bred in house or purchased from Jackson labs (10-12 weeks old; strain # 033076).
92 CD45.2 recipient mice were purchased from Taconic labs (10-12 weeks old; model # B6-M). IL-
93 $27R^{-/-}$ (Jackson labs; strain # 018078) were bred in house, as were IL-$27p28^{-/-}$ mice, originally
94 generated by Lexicon Pharmaceuticals, Inc. and previously described (Hall et al., 2012). IL-27-
95 p28-GFP reporters (Kilgore et al., 2018) were similarly bred in house, and the Procr-Ai6 was
96 generated from crossing the Procr-ERT2-cre line (Procr: Jacson labs; strain # 033052) which had
97 been backcrossed 9 generations onto the C57BL/6 background and was provided by Dr. Nancy
98 Speck to the Ai6 mouse line (Jackson labs; strain# 007906). Mice that contain a floxed allele of
99 the IL-27Rα (IL-$27R^{fl/fl}$) were provided by Dr. Booki Min (Do et al., 2017), and maintained within
100 our mouse colony. This line was then crossed with a CD4-cre mouse (Jackson labs; strain# 022071)
101 to generate the $CD4^{cre}$-IL-$27R^{flox/flox}$ mouse line. M1Red mice, which express red fluorescent

102 protein (RFP, encoded by *dsRed2*) under control of the *Irgm1* promoter, were received from
103 Gregory Taylor (Duke University) and maintained in-house. All mice were housed and bred in
104 specific pathogen-free (SPF) facilities in the Department of Pathobiology at the University of
105 Pennsylvania in accordance with institutional guidelines (IACUC# 805045). Cysts of ME49 strain
106 of *T. gondii* were collected from chronically infected CBA mice brain tissues. Experimental mice
107 were then infected i.p. with 20 cysts. For experiments where uninfected bone marrow was sorted,
108 a Prugniaud (PRU) strain of *T. gondii* expressing tdTomato was used (Pru-tdTomato). Both of
109 these are type II strains and show similar virulence.
110

111 **Functional Analysis of HSPC *in vivo***

112 For induction of the Procr-ERT2-cre, tamoxifen was given for three consecutive days (5
113 mg/mouse) prior to infection. For BRDU proliferation labeling, 5 mg of BRDU was given i.p. to
114 each mouse the same day as infection. 1mg/ml of BRDU was then provided in the drinking water
115 to mice throughout infection. To generate bone marrow chimeras, recipient mice were given a
116 radiation dose of 900-1000 rads at least 6 hrs. prior to transferring donor marrow. Donor marrow
117 was transferred (at least $2x10^6$ cells from each donor, unless otherwise stated; this resulted in a
118 total of $4x10^6$ cells being transferred for mixed chimeras) intravenously (i.v.) via retro-orbital
119 injection. Mice were then given 5 mL of Sulfamethoxazole/ Trimethoprim (200mg+40mg/5ml) in
120 their drinking water and replaced every 2-3 days for two weeks.
121

122 **Cell staining, flow cytometry, UMAP analysis, and detection of IL-27**

123 Splenocytes were obtained by grinding spleens through a 70 µm filter and washing with
124 RPMI supplemented with 5% fetal bovine serum (FBS). Red blood cells were then lysed by

125 incubating samples with ACK lysis buffer (Thermo Fischer Scientific) for 5 minutes before
126 washing again with RPMI + 5% FBS. Both femurs and tibias were harvested from mice for bone
127 marrow isolation. Connective tissue was removed from the bones by gentle scraping with a scalpel
128 before one end of each bone was cut off to expose the marrow. Bones were then placed in a 0.5 ml
129 microcentrifuge tube, with a hole punctured in the bottom with a 31g needle. The 0.5ml tube was
130 then placed within a 1.5 ml microcentrifuge tube; the nested tubes were then spun down at 13, 000
131 rcf for 1.5 min. The pelleted cells were then ACK lysed and washed as above (centrifuging at 500
132 rcf) before being passed through a 70 μm strainer and resuspended in appropriate media (adapted
133 from (Au - Amend et al., 2016)). For peritoneal exudate cells (PECs), 8 mL of PBS was injected
134 into the peritoneum of mice (21G needle attached to a 10 mL syringe) and re-aspirated using the
135 same needle and syringe. Syringe contents were then expelled into a 15 mL conical tube, spun
136 down at 300 rcf, and resuspended in appropriate media.

137 After cell numbers were determined for each sample, equivalent numbers of cells were
138 plated in a 96-well plate and spun down at 300 rcf. Cells were then washed with FACS Buffer [1x
139 PBS, 0.2% bovine serum antigen, 1mM EDTA] before incubating with Fc block [99.5 % FACS
140 Buffer, 0.5% normal rat serum, 1 μg/ml 2.4G2 IgG antibody] prior to staining. If CD16/32 was
141 stained for, the staining antibody was substituted for unconjugated 2.4G2 antibody in the Fc block.
142 Cells were stained with the viability dye Ghost Dye Violet 510 (Tonbo biosciences; 12-0870), and
143 the following antibodies were used for subsequent staining: CD90.2 (BD; clone 30-H12), B220
144 (BD; clone RA3-6B2), Ly6G (BD; clone 1A8), CD11b (BD; clone M1/70), Ly6C (Biolegend;
145 clone HK1.4), Sca-1 (BD/Invitrogen; clone D7), CD117/cKit (Biolegend; clone ACK2), CD135
146 (Biolegend; clone A2F10), CD150 (Biolegend; clone TC15-12F12.2), CD48 (Biolegend/BD;
147 clone HM48-1), CD127 (Biolegend; clone A7R34), CD16/32 (BD; clone 2.4G2), CD34

148 (Invitrogen; clone RAM34), CD115 (Biolegend; clone AFS98), CCR2 (Biolegend; clone
149 SA203G11), CX3CR1 (Biolegend; clone SA011F11), CD11c (Biolegend; clone N418), XCR1
150 (Biolegend; clone ZET), CD172a (Biolegend; clone P84), CD64 (Biolegend; clone X54-5/7.1),
151 F4/80 (Invitrogen; clone BM8), MHCII (Biolegend; clone M5/114.15.2), gp130 (Biolegend; clone
152 4H1B35), IL-27Rα (BD; 2918), CD132 (BD; clone 4G3), CD131 (BD; clone JORO50), IL-6Rα
153 (Biolegend; clone D7715A7), GM-CSFRα (R&D systems; clone 698423), CD210/IL-10R
154 (Biolegend; clone 1B1.3a), IFN-γR β (Biolegend; clone MOB-47), IFNAR-1 (Biolegend; clone
155 MAR1-5A3), IL-21R (Biolegend; clone 4A9), CD120a/TNFRI (Biolegend; clone 55R-286),
156 CD120b/TNFRII (Biolegend; clone TR75-89), and CD217/IL-17RA (Biolegend; clone
157 S19010F).

158 Intracellular staining for Ki67 (BD; clone B56), and BCL2 (Biolegend; clone BCL/10C4)
159 was performed using the Foxp3/Transcription Factor Staining Buffer Set (eBioscience) according
160 to the manufacturer's instructions. BRDU staining was done following a previous published
161 protocol (Matatall, Methods Mol. Biol., 2018). Cells within the vasculature were labeled by
162 injecting 3 μg of florescent anti-CD45 antibody (Biolegend; clone 30-F11)/mouse for 3 min prior
163 to euthanasia. Samples were run on a FACSymphony A3 or A5 (BD) and analyzed using the
164 FlowJo Software analysis program (TreeStar). For UMAP analyses, either 500 or 10,000 live cells
165 (for 5 days of culture or 10, respectively) per sample were sampled using the downsampling plug-
166 in (TreeStar) and subsequently concatenated. The concatenated samples were then used for UMAP
167 analysis with the FlowJo plug-in (TreeStar), using Euclidean distances with the nearest neighbor
168 set to 15, minimum distance of 0.5, and number of components set to 2. All compensated
169 parameters were then used in the analysis. After the UMAP analysis was performed, the X-shift

170 plug-in (TreeStar) was used to further analyze each cluster for its defining features (Samusik et al.,
171 2016).
172 For IL-27p28 detection, mouse IL-27p28/IL-30 Quantikine ELISA kit (M2728; R&D
173 Systems) was used according to the manufacturer's protocol.
174
175 **Immunofluorescence of bone marrow and image analysis**
176 Procr^{tdTomato}IL-27p28^{GFP} mice were generated, infected, and long bones harvested at 5 dpi.
177 The bones were then fixed in 4 % PFA for 2.5-4 hrs, washed with PBS 3x, and then decalcified in
178 0.5mM EDTA for ≥72 hrs before being paraffin embedded. 5 µm sections were taken and placed
179 onto charged microscope slides. For staining, slides were de-paraffinized, rehydrated, and placed
180 in 1mM EDTA (pH 8.0) overnight in a 55°C water bath to recover epitopes prior to staining. Slides
181 were washed in diH_2O the next day before proceeding with staining. Staining was adapted from
182 (Im et al., 2019). Slides were blocked with 100µl of blocking buffer (1x PBS+0.3% triton X-
183 100+1:200 rat IgG) for 30 min at room temperature. Slides were then washed 3x, for 5 min each
184 with PBS. Endogenous streptavidin and biotin were then blocked using the ReadyProbes
185 Stretavidin/Biotin Blocking solution (Invitrogen) according to the manufacturer's directions. After
186 washing, GFP was stained for at 1:40 with anti-GFP AF488 (Biolegend; FM264G) overnight at
187 4°C. Slides were washed 3x with PBS, as above, and then mounted and coverslipped using 15µl
188 Fluoro-Gel (Electron Microsopy Sciences). Slides were then imaged on a Stellaris Falcon (Leica)
189 microscope.
190 Images were processed and analyzed using the Fiji software package (Schindelin et al.,
191 2012). Images were converted to binary images, manually thresholded, watersheding applied to
192 separate overlapping objects, and positive cells counted using the "analyze particles" tool.

193

194 **Statistics**

195 An unpaired, Welch's t-test or one-way ANOVA with Sidak's correction for multiple
196 comparisons were used to test for significant differences between groups. These were used as
197 indicated in each figure and unless otherwise stated. P values of less that 0.05 were considered
198 significant.

199

200

201 **Results**

202 **IL-27 regulates monopoiesis during toxoplasmosis**

203 Infection with *T. gondii* leads to increased production of monocytes that is enhanced in the
204 absence of IL-27 (Aldridge et al., 2024), but it is unclear if this is a result of differentiation from
205 HSPCs or from the more differentiated monocyte progenitors (MPs). Therefore, the Procr-ERT2-
206 cre mouse line, which expresses Cre in HSPCs (Gur-Cohen et al., 2015; Iwasaki et al., 2010), was
207 crossed with the Ai6 reporter line to provide a lineage tracing model. In these mice, tdTomato is
208 expressed in *procr*$^+$ cells and, upon tamoxifen (TAM) treatment, HSPCs will be tdTomato$^+$ and
209 GFP$^+$ but their differentiated progeny will only express zsGreen (Fig. 1A). For these experiments,
210 Procr-Ai6 mice were treated with TAM, infected, and then at 5 dpi the BM and peripheral cells
211 were analyzed. Consistent with other HSPC lineage tracing models (Chapple et al., 2018; Säwen
212 et al., 2018), in naïve bone marrow only a small proportion (~5%) of long-term hematopoietic
213 stem cells (LTHSCs) were labeled which corresponded to a low proportion of zsGreen$^+$ monocytes
214 in the peritoneum and spleen (Fig. 1B-C). After infection, the proportion of zsGreen$^+$ LTHSCs in
215 the marrow nearly doubled (Fig. 1B), and the proportion of monocyte dendritic cell progenitors

216 (MDP) also increased (Supp Fig. 1A). This corresponded to an increase in labeled monocytes and
217 neutrophils in the bone marrow of infected mice (Supp. Fig. 1A). In the periphery, there was also
218 an increased proportion of zsGreen^{+} monocytes in the spleen, while in the peritoneum, the initial
219 site of infection and monocyte recruitment, the proportion of labeled monocytes reached ~100%
220 (Fig. 1C). These progenitors and their progeny were identified based on the expression of defining
221 surface markers as measured by flow cytometry (Supp. Fig. 2). Additional phenotyping revealed
222 that both classical (CCR2^{hi}, CX3CR1^{lo}) and non-classical (CCR2^{lo}, CX3CR1^{hi}) monocyte
223 population were labeled to equivalent degrees, indicating that infection impacts the recruitment of
224 both subsets (Supp. Fig 1B). These data sets indicate that the increased myelopoiesis that occurs
225 in response to infection with *T. gondii* is due to expansion and enhanced differentiation of HSPCs,
226 and not just MPs, into downstream progeny, eventually resulting in increased monocyte
227 production.

228 To determine the impact of IL-27 on this infection induced myelopoiesis, WT and IL-
229 27p28$^{-/-}$ mice were challenged with *T. gondii* and numbers of progenitors (from LTHSCs to MPs)
230 were analyzed (Fig. 1D). While infection led to an expansion of LTHSCs, the numbers of LTHSC,
231 granulocyte progenitors (GP), and other progenitors (including common lymphocyte progenitors
232 (CLPs), common myeloid progenitors (CMPs), and granulocyte monocyte progenitors (GMPs))
233 (data not shown) were not impacted by the absence of IL-27 (Fig. 1E). Infection also resulted in
234 a transient increase in MPs in WT mice, but in the absence of IL-27 this was enhanced at 3 and 5
235 dpi before returning to baseline at 10 dpi (Fig. 1F). A similar pattern was observed for the MDPs
236 (Supp. Fig. 1C), and in the IL-27p28$^{-/-}$ mice this corresponded to an increase in mature monocytes
237 in the liver (Supp. Fig. 1D). The CCR2^{hi}CX3CR1^{lo} phenotype of these cells indicated that these
238 were inflammatory monocytes, that were predominantly within the tissue parenchyma (Supp. Fig.

239 1E), suggesting that these monocytes are poised to participate in the tissue pathology associated
240 with these mice. This enhanced monocyte differentiation appeared independent of IFNγ, as
241 blockade of IL-27 during infection in IFNγ reporter mice showed no alteration in cytokine levels
242 in the bone marrow (Supp. Fig. 1F). Thus, one function of IL-27 during acute toxoplasmosis is to
243 limit monopoiesis and the generation of inflammatory monocytes.
244
245 **IL-27 regulates monocyte development in a cell intrinsic manner**
246 Previous studies have shown that during toxoplasmosis or trypanosomiasis the absence of
247 IL-27 results in enhanced $CD4^+$ T cell responses which contribute to increased accumulation of
248 inflammatory monocytes (Aldridge et al., 2024; Liu et al., 2021). To test if the early (5 dpi)
249 enhanced monopoiesis in the IL-$27^{-/-}$ mice observed here was a secondary consequence of the
250 $CD4^+$ T cell response, a $CD4^{cre}$ IL-$27R^{fl/fl}$ (CD4-IL-27R) mouse line was generated. In these mice
251 IL-27R expression was efficiently deleted in T cells, but other IL-27R expressing cells, such as B
252 cells, maintained expression (Supp. Fig. 3A). When infected with *T. gondii* these mice
253 phenocopied whole body IL-$27R^{-/-}$ mice and developed lethal immune pathology > 10 days post-
254 infection (data not shown). When control and CD4-IL-27R mice were infected and analyzed at 5
255 dpi there were equivalent numbers of monocyte progenitors (Fig. 2A). Thus, the enhanced
256 monopoiesis observed in the whole-body IL-$27p28^{-/-}$ mice is independent of the effect of IL-27 on
257 $CD4^+$ T cells.
258 Next, a mixed bone marrow chimera approach was used to determine if the enhanced
259 monopoiesis observed in the absence of IL-27 was cell intrinsic. In these experiments, WT and IL-
260 $27R^{-/-}$ marrow from naïve mice was used to generate a series of individual and mixed bone marrow
261 chimeras (Fig 2B). In the single-transfer chimeras, at fourteen weeks after reconstitution WT and

262 IL-27R$^{-/-}$ marrow reconstituted the hematopoietic system of irradiated recipients with 100% of
263 hematopoietic cells derived from the donor (Supp. Fig. 3B-C, left bars). In the mixed chimeras,
264 while initially no difference in chimerism was observed, as measured by output of peripheral T
265 and B cells, gradually there appeared to be decreased output from the IL-27R$^{-/-}$ lineage. This was
266 confirmed in the bone marrow where a reduced number of IL-27R$^{-/-}$ LTHSCs and downstream
267 MPs was observed (Supp. Fig. 3C, right bars, a 40:60 ratio KO: WT). Despite this reduction in the
268 IL-27R$^{-/-}$ LTHSCs, the population of CCR2^{hi}CX3CR1^{lo} monocytes in the periphery were
269 preferentially derived from the IL-27R$^{-/-}$ lineage (Supp. Fig. 3D, right bars, 60:40 ratio KO:WT).
270 To determine if infection would impact this differentiation, these mixed chimeras were infected
271 with *T. gondii* and analyzed at 5 dpi (Fig. 2C). After infection, IL-27R$^{-/-}$ LTHSC remained deficient
272 in the mixed chimeras, but MPs from both lineages were equivalent (Fig. 2C, right bars).
273 Additionally, the CCR2^{hi}CX3CR1^{lo} monocytes were still predominately derived from the IL-27R^{-}
274 $^{/-}$ lineage (Fig. 2D, right bars). Together, these data indicate that at homeostasis and during infection
275 IL-27 can support LTHSC populations but also temper the downstream processes that lead to
276 monocyte production. Additionally, this function is independent of IL-27 signals on CD4^{+} T cells,
277 but rather is due to a cell intrinsic ability of IL-27 to limit the production of inflammatory
278 monocytes.
279

280 **IL-27p28 is expressed in the bone marrow at homeostasis and during infection**

281 Given the impact of IL-27 on myelopoiesis described above, studies were performed to
282 characterize the cellular sources of IL-27p28 and their spatial location in the bone marrow of naïve
283 and infected mice. WT mice were infected, bone marrow harvested at 0, 3, 5, and 10 dpi, and local
284 production of the IL-27p28 subunit assayed (Fig. 3A). At 0 dpi, low constitutive levels of IL-27p28

285 were detected and increased throughout infection, with a peak at 5 dpi and elevated levels
286 maintained at 10 dpi (Fig. 3A). The use of an IL-27p28-GFP reporter mouse (Aldridge et al., 2024;
287 Kilgore et al., 2018) revealed a small population of p28-GFP^{+} cells in the bone marrow of naïve
288 mice, but by 5dpi this was expanded (Fig. 3B-C). Additional analysis of the bone marrow and
289 peripheral tissues (spleen, blood, PEC) (Fig. 3B-C) revealed that although a small proportion of T
290 cells were GFP^{+}, consistent with other reports (Kimura et al., 2016; Lin et al., 2023), monocytes
291 and macrophages were the dominant source of IL-27 in these sites, by proportion of GFP^{+} cells as
292 well as by cell number (Fig. 3B-C, Supp. Fig. 4A). Additionally, monocyte populations expressed
293 the highest levels of IL-27p28-GFP in comparison to other populations, such as dendritic cells
294 (Supp. Fig. 4B).

295 To visualize the spatial relationship between IL-27 expressing cells and HSPCs, femurs
296 from naive IL-27p28-GFP mice and imaged. In naïve mice, a stain for Sca-1 revealed low numbers
297 of HSPCs while p28^{GFP+} cells were present at a higher frequency; however, few of the cells in each
298 population colocalized (Supp. Fig. 4C, yellow arrows). During infection the expression of Sca-1
299 is upregulated by many cell populations (Baldridge et al., 2011; Morales-Mantilla et al., 2022),
300 and so the Procr$^{tdTomato+}$ cre reporter mouse (identifying HSPCs) was crossed with the IL-27p28^{GFP}
301 reporter. As HSCs are typically found within the hypoxic regions of the bone marrow (Eliasson
302 and Jönsson, 2010; Parmar et al., 2007), i.v. injection of anti-CD31 was used to label arterioles to
303 distinguish regions of the marrow that are highly vascularized or more hypoxic.
304 Immunofluorescence of the femur from 5 dpi highlighted that, similar to flow cytometric analysis
305 of the BM of the IL-27p28 reporters, infection resulted in increased numbers of p28^{GFP+} cells (Fig.
306 3D). Procr^{tdtomato} had a homogenous distribution in the femur (Supp. Fig. 4D, middle) whereas
307 p28^{GFP+} expression was more regional (Fig 3D; Supp. Fig. 4D, top). This was quantified by

308 sampling throughout the femur section (Fig 3D; Supp. Fig. 4D, regions 1-8). The area containing
309 almost exclusively Procr$^{tdTomato+}$ HSPCs, but few p28^{GFP+} cells, was an area of low vascularization,
310 consistent with the HSC niche (Fig. 3D; Supp. Fig. 4D, regions 3-5). However, in regions close to
311 the CD31^{+} vasculature, HSPCs and IL-27p28^{+} cells were found in proximity to one another (Fig.
312 3D; Supp. Fig. 4D, regions 1-2 and 6-8). When these regions were grouped based on this
313 vascularization, and GFP expressing cells normalized to tdTomato^{+} cells to account for potential
314 random distribution, a marked decrease in GFP^{+} cells was apparent in hypovascularized regions
315 (Fig. 3D). These data indicate that during infection the p28-GFP^{+} BM cells associate with HSPCs,
316 and this is most apparent near the vasculature and away from the HSC niche.
317

318 **Developmental expression of the IL-27R by hematopoietic cells**

319 The hematopoietic tree begins with undifferentiated LT-HSCs that differentiate into distinct
320 hematopoietic lineages and mature progeny; the color scheme in Fig. 4A reflects these
321 developmentally related populations. To determine which progenitor stages in the marrow were
322 responsive to IL-27, the expression of the IL-27Rα was compared with other cytokine receptors
323 (gp130, the IL-2R common gamma chain (CD132), IL-6Rα, and GM-CSFRα) that modulate
324 hematopoiesis (Collins et al., 2021; Reynaud et al., 2011). Expression of these receptors was
325 measured on HSPCs and committed progeny in naïve and infected mice (Fig. 4B-C; Fig. 5A-D).
326 The gp130 receptor, one chain of the IL-27 receptor that is also utilized by other IL-6 family
327 members, was expressed by all developmental stages examined in both naïve and infected mice
328 (Fig. 4B). In contrast, the IL-27Rα was highly expressed by LTHSCs, but markedly decreased
329 with lineage commitment, with mature neutrophils and monocytes showing no expression (Fig.
330 4C). The use of the Haemosphere RNA-seq data set (Choi et al., 2018) and the BloodSpot online

331 tool (Bagger et al., 2015) for the analysis of normal mouse hematopoietic bone marrow transcripts
332 (Chambers et al., 2007; Di Tullio et al., 2011) confirmed that levels of *IL27RA* mRNA were high
333 in LSKs and LTHSCs but decreased with lineage commitment (Supp. Fig. 5A-B). To determine
334 if IL-27R signaling was functional on HSPCs, bulk bone marrow was collected from M1Red
335 reporter mice (Pardy et al., 2024; Stifter et al., 2019), which express RFP under the control of the
336 *Irgm1* promoter, downstream of STAT1 signaling. When these cells were treated with IL-27 (an
337 activator of STAT1) the myeloid committed progenitors showed minimal RFP expression (Supp.
338 Fig. 5C), whereas HSPCS showed a time-dependent increase in reporter expression (Fig. 4D). This
339 differed dramatically from cells isolated *ex vivo* from IRGM1 reporter mice treated with another
340 activator of STAT1, the cytokine IFN-γ. After six hours, all hematopoietic progenitors analyzed
341 exhibited IRGM1-RFP expression (Supp. Fig. 5C and data not shown). The bulk BM cultures
342 stimulated with IL-27 also confirmed that known IL-27R expressing T, B, and NK cells within the
343 culture also responded to IL-27 with a similar kinetic of RFP activation to that of the HSPCs (Supp.
344 Fig. 5C).

345 When expression of the common IL-2R gamma chain (utilized by IL-2, -4, -7, -9, -15, and
346 -21), was analyzed, like gp130, it was ubiquitously expressed by all developmental stages,
347 although infection did upregulate its expression (Fig. 5A). Similarly, CD131, which is shared by
348 GM-CSF, IL-3, and IL-5 signaling, was expressed in most developmental stages and was markedly
349 enhanced upon infection (Fig. 5B). In contrast to the IL-27Rα, the expression of IL-6Rα and GM-
350 CSFRα by HSPCs was negligible, and the highest expression of these was detected on fully
351 committed, mature neutrophils and monocytes (Fig. 5C-D). Additionally, both the IL-6Rα and
352 GM-CSFRα showed enhanced expression during infection, further differing from IL-27Rα. A
353 summary of the survey for IL-10R, IFNγRβ, IFNαR, IL-17Rα, TNFIR, and TNFIIR is presented

354 in Supp. Fig. 6, and highlights that while some of these were constitutively expressed across
355 the hematopoietic tree, none of these receptors showed preferential expression by HSPCs.
356 Thus, this survey of cytokine receptor expression highlights that HSPCs but not downstream
357 progenitors are uniquely positioned to respond to IL-27.
358
359 **Infection derived IL-27 restrains a monocytic differentiation program in HSPCs**
360 To determine the impact of infection-driven IL-27 on HSPC differentiation, LTHSCs were
361 sorted from naïve or infected WT and IL-27R$^{-/-}$ mice at 5 dpi (see Supp. Fig. 7 for gating strategy).
362 These LTHSCs were then cultured in MethoCult and their phenotype and ability to form colonies
363 was quantified by morphology after 5 or 10 days of culture (Supp. Fig. 8). As expected, cells from
364 naïve mice generated all colony types, but in cultures derived from infected mice there were
365 reduced granulocyte/monocyte (GM) and granulocyte (G) colonies (Supp. Fig. 8A). However, by
366 10 days post-culture (dpc), there was a slight enhancement in macrophage/monocyte colonies (M)
367 from infected mice. The significant loss of colonies from infected mice, though, made
368 quantification of these colonies difficult. Thus, to better quantify these differences these cultures
369 were analyzed by flow cytometry to measure expression of canonical developmental markers (see
370 materials and methods). Dimensional reduction was then performed via UMAP, and cluster
371 formation was analyzed with X-shift to determine the dominant markers associated with individual
372 clusters. When cells were concatenated from all collection timepoints, 14 clusters were delineated
373 (Supp. Fig. 8B). These clusters where driven, predominantly, by either collection time (Supp. Fig.
374 8B, top) or proliferative status (Supp. Fig. 8B, bottom). Clusters 1-9 contained only samples from
375 5 dpc, and clusters 1-6 corresponded to undifferentiated, quiescent colonies that were minimally
376 proliferative (Ki67^{lo}) while clusters 7-9 were starting to proliferate (Ki67^{hi}) and differentiate to

377 give rise to mature cell populations. By 10 dpc, there was a loss of the quiescent colonies and a
378 rise of populations (clusters 10-14) that are Ki67^{hi} but have increased expression of mature myeloid
379 markers (CD11b, CD16/32, and Ly6C) (Supp. Fig. 8C). This reflects the increased differentiation
380 of colonies into mature myeloid cells. The UMAP analysis highlighted clusters 1, 6, 7, and 14 as
381 the dominant output of this assay (Supp. Fig. 8D): Cluster 1-undifferentiated progenitors (Ki67^{lo},
382 BCL2^{mid}, no other expression), Cluster 6-myeloid biased HSPCs (CD150^{hi}), Cluster 7- monocyte
383 progenitors (intermediate expression of myeloid markers (CD16/32^{lo}) , but expression of
384 progenitor markers (CD34^{int})), and cluster 14-mature monocyte (CD11b^{hi}, Ly6C^{hi}, CD16/32^{int})
385 (Supp. Fig. 8C). Furthermore, this clustering analysis highlighted that infection resulted in a loss
386 of myeloid progenitors (cluster 7) that was further reduced in the absence of IL-27 (Supp. Fig. 8E).
387 However, by 10 dpc this corresponded to enhanced differentiation into mature monocytes (cluster
388 14).

389 To compare the ability of HSPCs from WT or IL-27R$^{-/-}$ mice to generate monocyte
390 populations, cells solely from 10 dpc were clustered (Fig. 6A), with the dominant clusters being
391 1, 2, 3, 10, and 11 (Fig. 6B). Of these, HSPCs were present in cluster 1 (Sca-1^{+}cKit/CD117^{+}),
392 while cluster 10 contained monocyte progenitors (CD11b^{hi}Ly6C^{low}CD34^{+}CD115^{+}), and cluster 11
393 expressed markers of mature monocytes (CD11b^{hi}Ly6C^{+}) (Fig. 6C-D). Further analysis (Fig. 6E),
394 revealed that HSPCs from infected mice produced increased numbers of monocytes and
395 macrophages (cluster 11), but only HSPCs from infected, IL-27R$^{-/-}$ mice were enhanced in their
396 differentiation into monocyte progenitors (cluster 10). Thus, during infection the loss of IL-27
397 signaling enhances the skewing of HSPCs *ex vivo* toward monocyte differentiation.

398 In a complimentary *in vivo* approach, single transfers of WT or IL-27R$^{-/-}$ HSPCs from naïve
399 or infected mice were transferred into irradiated WT hosts and differentiation assessed (Fig. 6F).

400 For these experiments bulk marrow was utilized because, as discussed above, inflammation results
401 in upregulation of Sca-1 and other lineage defining markers (Baldridge et al., 2011; Morales-
402 Mantilla et al., 2022), making it difficult to define true HSPCs for transfer by cell-sorting. In
403 addition, for these studies mice were infected with a strain of *T. gondii* that expresses tdTomato
404 (Pru-tdTomato) (Christian et al., 2014; John et al., 2009) to allow parasite removal during sorting
405 and prevent infection of irradiated recipients. Analysis of spleens of recipient mice at 12 weeks,
406 revealed that donors from naive or infected IL-27R$^{-/-}$ mice produced a greater number of
407 monocytes than those derived from WT mice (Fig. 6F). These *ex vivo* and *in vivo* approaches
408 indicate that exposure of LTHSCs to IL-27 during infection results in a stable program that limits
409 monocyte production.
410
411 **IL-27 regulates the functionality and fitness of HSPCs during infection**
412 While the data sets presented above indicate a role for IL-27 in the regulation of HSPC
413 differentiation, it was unclear if loss of IL-27 signals during infection would affect their
414 functionality and fitness. To test if there were alteration in HSPC proliferation during infection,
415 WT and IL-27R$^{-/-}$ mice were treated with BRDU throughout infection and HSPC proliferation
416 analyzed at 5 dpi. The combination of Ki67 expression and BRDU incorporation was used to
417 distinguish HSPCs entering cell cycle (Ki67^{+}BRDU^{-}), cells that have entered cell cycle and are
418 actively proliferating (Ki67^{+}BRDU^{+}), and those that have proliferated but are no longer in cell
419 cycle (Ki67^{-}BRDU^{+}). In WT mice, the majority of LSKs are quiescent (Ki67^{-}BRDU^{-}), a proportion
420 of cells have entered cell cycle (Ki67^{+} BRDU^{-}), and a distinct Ki67^{+}BRDU^{+} population, as well as
421 a smaller Ki67^{-}BRDU^{+} population, can be detected. In the absence of IL-27 signaling, the most
422 prominent difference was a reduced proportion of Ki67^{+}BRDU^{+} cells (Fig. 7A). To determine if

423 this decreased Ki67^{+}BRDU^{+} population might be due to increased cell death of HSPCs in the IL-
424 27R$^{-/-}$ mice, cells were stained for Annexin V and a free-amine reactive viability dye to
425 discriminate early- and late-apoptotic cells as well as necrotic cells. No difference in cell death
426 was observed between WT and IL-27R$^{-/-}$ HSPCs (Supp. Fig. 9A). These data need to be interpreted
427 with care, as total HSPC numbers are not different between WT and IL-27$^{-/-}$ mice (see Fig 1), but
428 they suggest that IL-27 may regulate either the proliferation or retention of HSPCs within the bone
429 marrow niche.

430 A key feature of healthy HSCs is their ability to reconstitute the hematopoietic system of
431 irradiated mice, even after serial transfer (Siminovitch et al., 1964; Weissman, 2000). However,
432 inflammation and over-proliferation of HSCs can impair their ability to rescue lethally irradiated
433 recipients (Feng et al., 2008; King et al., 2011; Pietras et al., 2014). To test the impact of IL-27 on
434 HSC fitness and functionality, serial transplantations of HSCs from infected WT and IL-27R$^{-/-}$
435 mice were performed. In these experiments, marrow from naïve or infected donors was used to
436 produce single chimeras or to provide a 1:1 mix of WT and IL-27R$^{-/-}$ populations that were
437 transferred to irradiated recipients (Fig. 7B). All transfers promoted host survival and at 9 weeks
438 post-transplantation, the WT or IL-27R$^{-/-}$ donors from naïve and infected mice reconstituted the
439 blood compartment with a similar efficiency (Supp. Fig. 9C). However, in the 1:1 chimeras from
440 infected mice, the peripheral compartment was dominated by cells derived from WT mice.
441 Analysis of the marrow of the single transfer chimeras at 12 weeks post-transplant highlighted that
442 when donor cells were derived from infected mice there was a significant reduction in the numbers
443 of LTHSCs (Fig. 7C). To test the functionality of these HSCs, they were then transplanted for a
444 second time into irradiated hosts (Fig. 7D). Mice that received a secondary transplant of marrow
445 from naïve WT and IL-27R$^{-/-}$ mice survived irradiation, consistent with the ability of healthy HSCs

446 to undergo at least three rounds of transplantation (Siminovitch et al., 1964; Weissman, 2000).
447 Additionally, secondary transplantation of WT HSCs from infected mice also resulted in survival
448 of these hosts. However, the serial transfer of marrow from infected IL-27R$^{-/-}$ mice did not save
449 irradiated recipients (Fig. 7D). Thus, while IL-27R$^{-/-}$ HSPCs from infected mice maintain a
450 differentiation bias towards the monocyte lineage, they have a decreased survival and proliferation
451 capacity and a reduced ability to rescue irradiated mice.
452
453 **Discussion**
454 During toxoplasmosis, the increased production of inflammatory monocytes is critical to
455 control infection (Dunay et al., 2008), but these populations also have regulatory properties that
456 help to limit immune-pathology. For example, as infection progresses, the presence of IFN-γ in the
457 bone marrow promotes the production of monocytes that produce IL-10 and PGE_2 (Askenase et
458 al., 2015) which contribute to the restoration of homeostasis. Similarly, during toxoplasmosis and
459 other infections in response to IFN-γ/STAT1 signals (Furusawa et al., 2016 and our own
460 unpublished observations) monocytes become a dominant source of IL-27 (Detavernier et al.,
461 2019; Hall et al., 2012). While IL-27 has a critical role in directly limiting pathological T cell
462 responses, the data presented here show that IL-27 is also part of a regulatory loop that acts on
463 HSPCs to limit emergency myelopoiesis. Infection-induced monopoiesis gives rise to a population
464 of IL-27^{+} monocytes in the bone marrow that can then act on HSPCs to limit further monocyte
465 production. This observation is reminiscent of reports that IFN-γ activated
466 monocytes/macrophages can directly limit HSPCs (McCabe et al., 2015; Seyfried et al., 2020) or
467 the ability of IL-10 to limit emergency myelopoiesis in the fetus (Collins et al., 2024). Likewise,
468 during infection with *T. gondii*, Tregs (Glatman Zaretsky et al., 2017) appear to participate in a

469 regulatory cross-talk with HSPCs. A better understanding of how immune cells in the bone
470 marrow, such as memory B and T, influence HSPCs is needed.

471 One challenge that faces HSCs during inflammation is the need to protect from stressors
472 associated with proliferation that adversely affect the functions of these cells (Caiado et al., 2021).
473 The concept of HSC "exhaustion" has been developed to describe HSCs that are no longer able to
474 fulfill their role in proliferation and reconstitution of steady-state hematopoiesis (Singh et al., 2020;
475 Zhao and Deininger, 2023). Unanticipated findings from our studies here were the reduced ability
476 of IL-27R$^{-/-}$ HSCs post-infection to compete with WT HSCs, as well as the inability of these HSCs
477 to reconstitute upon secondary transfer, hallmarks of functional exhaustion (Singh et al., 2020).
478 These results infer that the ability of IL-27 to limit emergency myelopoiesis is also associated with
479 the ability of IL-27 to limit HSC exhaustion. It is important to note, however, that these studies
480 indicate that multiple cells within the HSPC category, including MPPs, express the IL-27Rα and
481 are responsive to IL-27. Whether the impacts on HSC exhaustion detected here are due to the direct
482 effects of IL-27 on HSCs or on downstream MPPs, then, warrants further investigation. Aberrant
483 HSPC responses are associated with conditions such as clonal hematopoiesis and aging, and there
484 has been interest in the development of strategies to target these HSPCs. Thus, selective targeting
485 and depletion of "aged" HSPCs via anti-CD150 treatments has been reported to restore balanced
486 hematopoietic output and "youthful" blood phenotypes (Ross et al., 2024). Whether IL-27
487 treatment can be used to preserve HSPCs, or be blocked to enhance monocyte production, remains
488 to be tested.

489 A common feature of certain models of trained immunity that affect hematopoiesis is that
490 cytokines, such as IFN-γ and IL-6, promote long term changes that polarize HSPCs toward
491 myeloid differentiation (Cheong et al., 2023; Kaufmann et al., 2018; Khan et al., 2020). Inherent

492 in this process is the idea that HSCs or downstream progeny would be sensitive to different
493 cytokines. The ability to survey the expression of cytokine receptors that influence hematopoiesis
494 emphasized that the shared cytokine receptor chains gp130 and IL-2Rγ are uniformly
495 expressed throughout hematopoietic development. In contrast, the alpha chain receptors for
496 individual cytokines (IL-6Rα, GM-CSFRα, IL-10R, IFNγRβ, IFNAR, IL-21R, TNFRI, and
497 TNFRII) displayed a much more restricted pattern of expression that correlated with key
498 features of the biology of individual cytokines. For example, the limited expression of the IL-
499 6 receptor on downstream progeny is consistent with reports of its high expression on MPPs
500 but not on HSCs (Mirantes et al., 2014; Reynaud et al., 2011). Nevertheless, that HSCs express
501 high levels of the IL-27R, which decreases with differentiation, emphasizes that these stem
502 cells are especially sensitive to the effects of IL-27. Whether IL-27 tempers some of the
503 processes associated with innate training or is itself associated with long-term epigenetic
504 changes is the subject of ongoing studies.

505 The use of murine models of toxoplasmosis have revealed many of the inhibitory
506 activities of IL-27, and the datasets presented here highlight the ability of IL-27 to influence
507 HSPCs to restrain monocyte/macrophage induction. There are also reports during other
508 infections and models that show IL-27 can regulate neutrophil and monocyte development
509 (Furusawa et al., 2016; Liu et al., 2014; Liu et al., 2021; Seita et al., 2008; Sun et al., 2017; Wirtz
510 et al., 2006). For example, during infection with an attenuated strain of *Plasmodium berghei,* IL-
511 27 was required for the induction of a neutrophil response, and *in vitro* IL-27 blunted the ability
512 of HSPCs to differentiate into the macrophage lineage (Furusawa et al., 2016). However, in less
513 inflammatory settings, such as tumor growth, the overexpression of IL-27 resulted in LSK
514 expansion and the induction of an M1 macrophage population (Zhu et al., 2023). Likewise, in a

515 model of angiotensin-mediated atherosclerosis, IL-27 was needed to overcome HSC quiescence
516 and increase differentiation and output of mature myeloid cells (Peshkova et al., 2019). While it
517 can be difficult to ascribe some of these effects to IL-27 acting directly on HSC, the contrasting
518 nature of these data sets suggest that the impact of IL-27 on HSPCs is context dependent. Indeed,
519 reports that TNFα can upregulate HSPC expression of the IL-27R (He et al., 2020) suggests that
520 IL-27 responsiveness can be regulated by the local environment. A better appreciation of these
521 environmental signals at homeostasis and during different types of inflammation, then, should help
522 to define these context-dependent activities of IL-27 on hematopoiesis.
523

524 **Acknowledgments and funding**

525 We would like to thank Dr. Nancy Speck for generously providing us with the Procr-cre
526 mouse line. Additionally, we thank Dr. Gordon Ruthel for his assistance and instruction in
527 capturing images of the mouse bone marrow. Schematic were created using BioRender (agreement
528 license BU27RCNPBH).

529 Funding for this work was provided by the NIH equipment grant (S10 OD032305-01A1),
530 NIH fellowship support (F31 AI 161962-03), and the Emmerson Foundation.
531
532

533 **Figure legends**

534 **Figure 1. IL-27 regulates monopoiesis during infection.** A) Schematic of infection and TAM
535 dosing strategy for Procr-Ai6 mice. B) Procr-Ai6 mice were infected and representative flow plots
536 of LTHSCs (Lin (CD3, NK1.1, B220, Ly6G)$^{-}$, Sca-1^{+}, CD117 (cKit)$^{+}$, CD135^{-}, CD48^{-}, CD150^{+})
537 from naïve (left) and infected (right) mice are shown. Proportions of zsGreen^{+} LTHSCs were then

538 quantified in both groups. C) Proportions of zsGreen^{+} monocytes (CD3^{-}, B220^{-}, CD11b^{+}, Ly6C^{+},
539 Ly6G^{-}) in the spleen and PECs of naïve and infected mice. D) Schematic of infection of WT and
540 IL-27p28$^{-/-}$ mice for E-F. E) Numbers of LTHSCs and granulocyte progenitors (GPs) (CD3^{-},
541 NK1.1^{-}, B220^{-}, CD117^{+}, CD34^{+}, CD16/32^{hi}, Ly6C^{+}, CD135^{-}, CD115^{-}) in the bone marrow of WT
542 and IL-27p28$^{-/-}$ infected mice throughout infection. F) Monocyte progenitors (MPs) (CD3^{-}, NK1.1^{-}
543 , B220^{-}, CD117^{+}, CD34^{+}, CD16/32^{hi}, Ly6C^{+}, CD135^{-}, CD115^{+}; orange box) in the bone marrow
544 of infected WT and IL-27p28$^{-/-}$ mice throughout infection. Representative flow plots are shown
545 (left) and quantified (right). Statistical significance was tested by one-way ANOVA with Sidak's
546 correction. *, **, and *** correspond to p-values ≤ 0.05, 0.01, and 0.001, respectively. N=3-5
547 mice/group and data shown are representative of 2-3 experiments.
548
549 **Supplemental Figure 1. IL-27 regulates monopoiesis during infection.** A) The proportion of
550 zsGreen^{+} monocyte dendritic cell progenitors (MDPs) (CD3^{-}, NK1.1^{-}, B220^{-}, CD117^{+}, CD34^{+},
551 CD16/32^{lo}, CD115^{+}), monocytes, and neutrophils (CD3^{-}, B220^{-}, CD11b^{+}, Ly6C^{+}, Ly6G^{+}) in the
552 BM of naïve and infected Procr-Ai6 mice. B) The proportion of zsGreen^{+} CCR2$^{hi/lo}$ CX3CR1$^{hi/lo}$
553 monocytes in the spleen and PECs in naïve and infected Procr-Ai6 mice. C) Number of MDPs in
554 WT and IL-27p28$^{-/-}$ mice in the bone marrow during infection. D) Numbers of monocytes in the
555 liver in WT and IL-27p28$^{-/-}$ throughout infection. E) WT and IL-27p28$^{-/-}$ mice were injected I.V.
556 with fluorescent anti-CD45 to label immune cells in the vasculature. Numbers of I.V. label^{-} and
557 CCR2^{hi}CX3CR1^{lo} monocytes in the liver were then quantified throughout infection. F) IFNγ-
558 Thy1.1 reporter mice were infected and treated with an anti-p28 blocking antibody. Numbers of
559 IFNγ^{+} cells in the bone marrow was then assessed by flow cytometry. Representative flow plots
560 are shown (left) and quantified (right). Statistical significance was tested by one-way ANOVA with

561 Sidak's correction. *, **, and *** correspond to p-values ≤ 0.05, 0.01, and 0.001, respectively.
562 N=3-5 mice/group and data shown are representative of 2-3 experiments.
563
564 **Supplemental Figure 2. Gating strategy for flow cytometric analysis of cells in the bone**
565 **marrow and periphery.** Representative flow plots from the bone marrow (top) and spleen
566 (bottom) are shown indicating the gating strategy used to identify various cell populations. The
567 combination of surface markers used are listed in the tables (bottom) and are color coded to
568 correspond to both the developmental schematic pictured as well as the corresponding flow gate
569 on the representative plots.
570
571 **Figure 2. IL-27 regulates monopoiesis during infection in a cell intrinsic manner.** A) CD4-IL-
572 27R mice were infected and MPs (orange box) measured at 5 dpi in the BM. Representative flow
573 plots are shown (left) and quantified (right). B) Schematic of BM chimeras generated from WT
574 (CD45.1) and IL-27R$^{-/-}$ (CD45.1.2) bulk bone marrow that were then infected and used in C-D. C)
575 The proportion of LTHSCs (left) and MPs (right) from each respective donor lineage in the bone
576 marrow of both the single (left two bars) and mixed (right two bars) chimeras at 5 dpi. D)
577 Representative flow plots pre-gated on splenic monocytes (left plot) and then down-gated on
578 CCR2^{hi}CX3CR1^{lo} (right plot) monocytes at 5 dpi. WT derived monocytes are shown in the solid-
579 dark gray while IL-27R$^{-/-}$ derived cells are in the dashed-light gray. The proportion of each donor
580 lineage that contribute to mature CCR2^{hi}CX3CR1^{lo} splenic monocytes at 5 dpi were then
581 quantified (far right). Statistical significance was tested by either Welch's T-test (A) or one-way
582 ANOVA with Sidak's correction (C-D). *, **, and *** correspond to p-values ≤ 0.05, 0.01, and
583 0.001, respectively. N=3-5 mice/group and data shown are representative of 2-3 experiments.

584

585

586 **Supplemental Figure 3. IL-27 regulates monopoiesis during infection and post-irradiation in**
587 **a cell intrinsic manner.** A) IL-27Rα expression on $CD4^+$ ($CD19^-CD3^+CD8\alpha^-$) T cells, $CD8^+$
588 ($CD19^-CD3^+CD4^-$) T cells, and B cells ($CD19^+CD3^-$) in CD4-27R mice at 5 dpi. B) Reconstitution
589 and chimerism in the peripheral blood 1:1 WT:IL-$27R^{-/-}$ chimeras was measures over time. T (top)
590 and B (bottom) cells from each lineage are shown. C) The proportion of LTHSCs (left) and MPs
591 (right) from each respective donor lineage in the bone marrow post-reconstitution and pre-
592 infection. D) The proportion of $CCR2^{hi}CX3CR1^{lo}$ monocytes from each respective donor lineage
593 in the spleen and liver post-reconstitution and pre-infection. Statistical significance was tested by
594 one-way ANOVA with Sidak's correction. *, **, and *** correspond to p-values ≤ 0.05, 0.01, and
595 0.001, respectively. N=3-5 mice/group and data shown are representative of 2 repeated
596 experiments.

597

598 **Figure 3. IL-27p28 is produced in the BM during infection.** A) WT mice were infected, and the
599 bone marrow harvested throughout infection. BM was either washed with media or cultured for
600 24 hrs. and supernatant collected. Both the wash and supernatant were analyzed by ELISA for IL-
601 27p28. B) IL-27p28-GFP reporter mice were infected and their bone marrow analyzed by flow
602 cytometry throughout infection. A representative flow plot at 5 dpi of bulk marrow is shown (left)
603 and proportion of immune cell contribution to the GFP^+ population measured (right). C) Numbers
604 of IL-27p28-GFP^+ cells in the spleen, blood, and BM of infected mice were quantified throughout
605 infection (left). Proportions of GFP^+ $CD45^+$ cells were analyzed by cell type in the blood, spleen,
606 and PEC during infection (left). D) Femurs from infected Procr-$tdTomato^+$p28-GFP^+ mice were

607 harvested, sectioned, and imaged at 40x magnification. The total imaged femur is shown (top),
608 with zoomed in sections shown below for increased detail of cellular localization (bottom). Arrows
609 indicate areas of localization with Procr-tdTomato$^+$ and p28-GFP$^+$ cells. Numbers of Procr-
610 tdTomato$^+$ and p28-GFP$^+$ cells were then counted in eight randomly selected regions throughout
611 the marrow (see Supp. Fig. 4). GFP$^+$ cells were normalized to tdTomato$^+$ cells and the eight counted
612 regions classified as areas of hyper- or hypo-vascularization according to proximity of the region
613 to the labeled vasculature. This allowed quantification of the localization of cells (bottom right).
614
615 **Supplemental Figure 4. IL-27p28 is produced in the bone marrow during infection.** A) IL-
616 27p28-GFP mice were infected, and the numbers of each CD45$^+$, immune cell type that expressed
617 GFP in the BM or periphery quantified throughout infection. B) Levels of IL-27p28-GFP
618 expression were measured in bulk monocytes (red) and dendritic cells (blue) in the bone marrow
619 (left) and spleen (right). C) Femurs from naïve IL-27p28-GFP mice were stained for Sca-1 and
620 imaged at 40x magnification. Zoomed in images are shown (right) of the indicated areas, with the
621 yellow arrows indicating positively stained, Sca-1$^+$ cells. D) The merged image shown in Fig. 3D
622 is separated by channel (GFP, tdTomato, and AF647, from top to bottom). Eight randomly selected
623 regions that were used for quantification of either GFP$^+$ or tdTomato$^+$ cells are shown (top), and
624 the quantification of cells in each region is shown next to the corresponding florescence channel
625 (right).
626
627 **Figure 4. Expression of the IL-27R subunits gp130 and IL-27Rα during hematopoietic**
628 **development.** A) Schematic ball-and-stick model of hierarchical hematopoietic development. Cell
629 type colors are maintained for reference in the following panels. B) Progenitors and progeny shown

630 in (A) were analyzed in WT and infected mice (at 5 dpi) by flow cytometry for the gp130 receptor.
631 10,000 live cells were concatenated from n=3 mice, and representative flow plots are shown. The
632 fold change of the MFI of the receptor in each cell type over the FMO control for that cell type
633 was then quantified. C) Cells in (B) were analyzed for expression of the IL-27Rα and analyzed as
634 above. D) Bulk bone marrow was isolated from IRGM1-dsRed reporter mice. 22 x 10^6 cells were
635 plated per condition and stimulated with 20 ng/ml of IL-27 for 0, 6, or 48 hours and RFP expression
636 measured by flow cytometry.
637
638 **Supplemental Figure 5. IL-27Rα transcript expression during hematopoiesis and differential**
639 **sensitivity of LTHSC and CMP to IL-27.** A) Expression levels of *IL27RA* are shown from the
640 Haemosphere RNA-seq data set and online tool as well as the Blood Spot data set and visualizer
641 (B). C) Representative flow plots of IRGM1-RFP expression in LTHSCs, CMPs, and lin^+ T, NK,
642 and B cells 48 hrs. post-stimulation with IL-27 are shown (top). *In vivo* treatment of IRGM1-RFP
643 reporter mice with 1 μg of recombinant IFNγ was performed and all populations analyzed as in
644 (C). Representative flow plots are shown.
645
646 **Figure 5. Developmental expression of hematopoietic cytokine receptors.** A) Expression of
647 CD132 (IL-2Rγ) and B) CD131 (GM-CSF/IL-3/IL-5Rβ) was analyzed by flow cytometry on
648 progenitors and progeny in the BM of naïve and 5 dpi mice as in Fig. 4. C) Expression of IL-6Rα
649 and D) GM-CSFRα were measured as in (A).
650
651 **Supplemental Figure 6. Developmental expression of additional cytokine receptors.** Indicated
652 cytokine receptors were analyzed in naive and infected mice as described in Fig. 4-5.

653

654 **Figure 6. IL-27 limits infection induced HSPC polarization.** WT and IL-27R$^{-/-}$ mice were
655 infected for 5 days, LTHSCs sorted, and cultured in MethoCult for 10-12 days before being
656 analyzed by flow cytometry. A) 10,000 live cells from n=3-4 mice/ group (WT (naïve+5 dpi) and
657 IL-27R$^{-/-}$ (5 dpi)) were concatenated and dimensionally reduced via UMAP. B) Numbers of cells
658 in each cluster from (A) were measured. C) X-shift analysis was used to identify the expression
659 level of each marker used in the clustering performed in (A). 5 of the dominant clusters from (B)
660 are shown. D) Clusters 1, 10, and 11, all involved in monocyte development, are highlighted. E)
661 Contribution of Clusters 1, 10, and 11 to each genotype are shown (left) and quantified (right). F)
662 Single bone marrow chimeras were generated from infected WT and IL-27R$^{-/-}$ mice or naïve
663 controls (left). The numbers of single-donor derived, mature monocytes were then measured at 14
664 weeks post-transplant and compared based on WT vs IL-27R$^{-/-}$ donor (right). Statistical
665 significance was tested by one-way ANOVA with Sidak's correction. *, ***, and **** correspond
666 to p-values $\leq$ 0.05, 0.001, and 0.0001, respectively. N=3-5 mice/group and data shown are
667 representative of 2-3 repeated experiments.

668

669 **Supplemental Figure 7. Gating strategy for sorting of LTHSCs used in monocyte**
670 **differentiation.** LTHSCs were sorted from WT naïve, WT 5 dpi, and IL-27R$^{-/-}$ 5 dpi mice. The
671 gating strategy is shown as well as the purity of sorted samples (last panel).

672

673 **Supplemental Figure 8. Development and validation of an unbiased flow cytometry approach**
674 **for the analysis of MethoCult colonies.** WT and IL-27R$^{-/-}$ mice were infected, LTHSCs sorted
675 and cultured in MethoCult for either 5 or 10 days. A) Colony phenotypes were analyzed by

676 microscopy and counted by eye. B) Colonies were collected at either 5 or 10 days post-culture
677 (dpc) and analyzed by flow cytometry. 500 live cells from n=3-4 mice/ group were concatenated
678 and dimensionally reduced via UMAP. UMAP plots are shown, and Ki67 expression is overlayed.
679 C) X-shift analysis was used to identify the expression level of each marker used in the clustering
680 performed in (B). D) Numbers of cells in each cluster from (B) were measured. E) Contribution of
681 each genotype to each cluster was quantified. Statistical significance was tested by one-way
682 ANOVA with Sidak's correction. *, ***, and **** correspond to p-values ≤ 0.05, 0.001, and
683 0.0001, respectively. N=3-4 mice/group and data shown are from 1 of 3 experiments.
684
685 **Figure 7. Testing the impact of IL-27 on functionality and fitness of HSPCs during infection.**
686 A) WT and IL-27R$^{-/-}$ were infected, treated with 5 mg BRDU, and kept on 1mg/ml BRDU in the
687 drinking water throughout infection. Incorporation of BRDU was then measured in Lin^{-}Sca-
688 1^{+}cKit^{+} (LSK) progenitor cells in comparison to Ki67 at 5 dpi. Representative flow plots are shown
689 (left) and the proportion of BRDU^{+}Ki67^{+} cells quantified (right). B) Schematic for the generation
690 of BM chimeras from infected mice used in (C). C) As in Fig. 6F, numbers of LTHSCs from
691 recipients receiving single-transfer donor marrow from either uninfected or infected mice were
692 measured based on genotype. D) Secondary transplant chimeras from mice that originally received
693 naïve or infected marrow where generated as shown (left). Survival of recipients was then assessed
694 (right).
695
696 **Supplemental Figure 9. Testing HSPC survival and fitness.** A) FMO gating controls for Ki67
697 and BRDU in the LSK population corresponding to Fig. 7A. B) LTHSCs from WT and IL-27R$^{-/-}$
698 BM at 5 dpi was stained for Annexin V (AV) expression and free-amine staining viability dye

699 (LD). This allowed the measurement of apoptotic (AV^+LD^-), late apoptotic (AV^+LD^+), and necrotic
700 (AV^-LD^+) cells. The proportion of LTHSCs in each of these stages was quantified. C) Monocyte
701 genotype was analyzed at 9 weeks post-transplant (wpt) from either naïve WT (CD45.1) or IL-
702 $27R^{-/-}$ (CD45.1.2) donors (top) or from infected donors (bottom), including a 1:1 mix of infected
703 WT and IL-$27R^{-/-}$ donors. Statistical significance was tested by Welch's t-test.

704

705

706 **References**

707 Aldridge, D.L., D. Moodley, J. Park, A.T. Phan, M. Rausch, K.F. White, Y. Ren, K. Golin, E. Radaelli, R.
708 Kedl, P.M. Holland, J. Hill, and C.A. Hunter. 2024. Endogenous IL-27 during toxoplasmosis
709 limits early monocyte responses and their inflammatory activation by pathological T cells.
710 *mBio* 15:e0008324.
711 Askenase, M.H., S.J. Han, A.L. Byrd, D. Morais da Fonseca, N. Bouladoux, C. Wilhelm, J.E. Konkel,
712 T.W. Hand, N. Lacerda-Queiroz, X.Z. Su, G. Trinchieri, J.R. Grainger, and Y. Belkaid. 2015.
713 Bone-Marrow-Resident NK Cells Prime Monocytes for Regulatory Function during
714 Infection. *Immunity* 42:1130-1142.
715 Au - Amend, S.R., K.C. Au - Valkenburg, and K.J. Au - Pienta. 2016. Murine Hind Limb Long Bone
716 Dissection and Bone Marrow Isolation. *JoVE* e53936.
717 Bagger, F.O., D. Sasivarevic, S.H. Sohi, L.G. Laursen, S. Pundhir, C.K. Sønderby, O. Winther, N. Rapin,
718 and B.T. Porse. 2015. BloodSpot: a database of gene expression profiles and transcriptional
719 programs for healthy and malignant haematopoiesis. *Nucleic Acids Research* 44:D917-
720 D924.
721 Baldridge, M.T., K.Y. King, N.C. Boles, D.C. Weksberg, and M.A. Goodell. 2010. Quiescent
722 haematopoietic stem cells are activated by IFN-gamma in response to chronic infection.
723 *Nature* 465:793-797.
724 Baldridge, M.T., K.Y. King, and M.A. Goodell. 2011. Inflammatory signals regulate hematopoietic
725 stem cells. *Trends Immunol* 32:57-65.
726 Caiado, F., E.M. Pietras, and M.G. Manz. 2021. Inflammation as a regulator of hematopoietic stem
727 cell function in disease, aging, and clonal selection. *Journal of Experimental Medicine* 218:
728 Chambers, S.M., N.C. Boles, K.Y. Lin, M.P. Tierney, T.V. Bowman, S.B. Bradfute, A.J. Chen, A.A.
729 Merchant, O. Sirin, D.C. Weksberg, M.G. Merchant, C.J. Fisk, C.A. Shaw, and M.A. Goodell.
730 2007. Hematopoietic fingerprints: an expression database of stem cells and their progeny.
731 *Cell Stem Cell* 1:578-591.
732 Chapple, R.H., Y.J. Tseng, T. Hu, A. Kitano, M. Takeichi, K.A. Hoegenauer, and D. Nakada. 2018.
733 Lineage tracing of murine adult hematopoietic stem cells reveals active contribution to
734 steady-state hematopoiesis. *Blood Adv* 2:1220-1228.

735 Cheong, J.G., A. Ravishankar, S. Sharma, C.N. Parkhurst, S.A. Grassmann, C.K. Wingert, P. Laurent,
736 S. Ma, L. Paddock, I.C. Miranda, E.O. Karakaslar, D. Nehar-Belaid, A. Thibodeau, M.J. Bale,
737 V.K. Kartha, J.K. Yee, M.Y. Mays, C. Jiang, A.W. Daman, A. Martinez de Paz, D. Ahimovic, V.
738 Ramos, A. Lercher, E. Nielsen, S. Alvarez-Mulett, L. Zheng, A. Earl, A. Yallowitz, L. Robbins,
739 E. LaFond, K.L. Weidman, S. Racine-Brzostek, H.S. Yang, D.R. Price, L. Leyre, A.F. Rendeiro,
740 H. Ravichandran, J. Kim, A.C. Borczuk, C.M. Rice, R.B. Jones, E.J. Schenck, R.J. Kaner, A.
741 Chadburn, Z. Zhao, V. Pascual, O. Elemento, R.E. Schwartz, J.D. Buenrostro, R.E. Niec, F.J.
742 Barrat, L. Lief, J.C. Sun, D. Ucar, and S.Z. Josefowicz. 2023. Epigenetic memory of
743 coronavirus infection in innate immune cells and their progenitors. *Cell* 186:3882-
744 3902.e3824.
745 Choi, J., T.M. Baldwin, M. Wong, J.E. Bolden, K.A. Fairfax, E.C. Lucas, R. Cole, C. Biben, C. Morgan,
746 K.A. Ramsay, A.P. Ng, M. Kauppi, L.M. Corcoran, W. Shi, N. Wilson, M.J. Wilson, W.S.
747 Alexander, D.J. Hilton, and C.A. de Graaf. 2018. Haemopedia RNA-seq: a database of gene
748 expression during haematopoiesis in mice and humans. *Nucleic Acids Research* 47:D780-
749 D785.
750 Christian, D.A., A.A. Koshy, M.A. Reuter, M.R. Betts, J.C. Boothroyd, and C.A. Hunter. 2014. Use of
751 transgenic parasites and host reporters to dissect events that promote interleukin-12
752 production during toxoplasmosis. *Infect Immun* 82:4056-4067.
753 Collins, A., C.A. Mitchell, and E. Passegué. 2021. Inflammatory signaling regulates hematopoietic
754 stem and progenitor cell development and homeostasis. *Journal of Experimental Medicine*
755 218:
756 Collins, A., J.W. Swann, M.A. Proven, C.M. Patel, C.A. Mitchell, M. Kasbekar, P.V. Dellorusso, and E.
757 Passegué. 2024. Maternal inflammation regulates fetal emergency myelopoiesis. *Cell*
758 187:1402-1421.e1421.
759 Detavernier, A., A. Azouz, H. Shehade, M. Splittgerber, L. Van Maele, M. Nguyen, S. Thomas, Y.
760 Achouri, D. Svec, E. Calonne, F. Fuks, G. Oldenhove, and S. Goriely. 2019. Monocytes
761 undergo multi-step differentiation in mice during oral infection by Toxoplasma gondii.
762 *Commun Biol* 2:472.
763 Di Tullio, A., T.P. Vu Manh, A. Schubert, G. Castellano, R. Månsson, and T. Graf. 2011.
764 CCAAT/enhancer binding protein alpha (C/EBP(alpha))-induced transdifferentiation of
765 pre-B cells into macrophages involves no overt retrodifferentiation. *Proc Natl Acad Sci U S*
766 *A* 108:17016-17021.
767 Do, J., D. Kim, S. Kim, A. Valentin-Torres, N. Dvorina, E. Jang, V. Nagarajavel, T.M. DeSilva, X. Li,
768 A.H. Ting, D.A.A. Vignali, S.A. Stohlman, W.M. Baldwin, 3rd, and B. Min. 2017. Treg-specific
769 IL-27Rα deletion uncovers a key role for IL-27 in Treg function to control autoimmunity.
770 *Proc Natl Acad Sci U S A* 114:10190-10195.
771 Dunay, I.R., R.A. Damatta, B. Fux, R. Presti, S. Greco, M. Colonna, and L.D. Sibley. 2008. Gr1(+)
772 inflammatory monocytes are required for mucosal resistance to the pathogen Toxoplasma
773 gondii. *Immunity* 29:306-317.
774 Eliasson, P., and J.I. Jönsson. 2010. The hematopoietic stem cell niche: low in oxygen but a nice
775 place to be. *J Cell Physiol* 222:17-22.
776 Feng, C.G., D.C. Weksberg, G.A. Taylor, A. Sher, and M.A. Goodell. 2008. The p47 GTPase Lrg-47
777 (Irgm1) Links Host Defense and Hematopoietic Stem Cell Proliferation. *Cell Stem Cell* 2:83-
778 89.

779 Findlay, E.G., R. Greig, J.S. Stumhofer, J.C. Hafalla, J.B. de Souza, C.J. Saris, C.A. Hunter, E.M. Riley,
780 and K.N. Couper. 2010. Essential role for IL-27 receptor signaling in prevention of Th1-
781 mediated immunopathology during malaria infection. *J Immunol* 185:2482-2492.
782 Furusawa, J., I. Mizoguchi, Y. Chiba, M. Hisada, F. Kobayashi, H. Yoshida, S. Nakae, A. Tsuchida, T.
783 Matsumoto, H. Ema, J. Mizuguchi, and T. Yoshimoto. 2016. Promotion of Expansion and
784 Differentiation of Hematopoietic Stem Cells by Interleukin-27 into Myeloid Progenitors to
785 Control Infection in Emergency Myelopoiesis. *PLoS Pathog* 12:e1005507.
786 Glatman Zaretsky, A., C. Konradt, F. Dépis, J.B. Wing, R. Goenka, D.G. Atria, J.S. Silver, S. Cho, A.I.
787 Wolf, W.J. Quinn, J.B. Engiles, D.C. Brown, D. Beiting, J. Erikson, D. Allman, M.P. Cancro, S.
788 Sakaguchi, L.F. Lu, C.O. Benoist, and C.A. Hunter. 2017. T Regulatory Cells Support Plasma
789 Cell Populations in the Bone Marrow. *Cell Rep* 18:1906-1916.
790 Gur-Cohen, S., T. Itkin, S. Chakrabarty, C. Graf, O. Kollet, A. Ludin, K. Golan, A. Kalinkovich, G.
791 Ledergor, E. Wong, E. Niemeyer, Z. Porat, A. Erez, I. Sagi, C.T. Esmon, W. Ruf, and T. Lapidot.
792 2015. PAR1 signaling regulates the retention and recruitment of EPCR-expressing bone
793 marrow hematopoietic stem cells. *Nat Med* 21:1307-1317.
794 Hall, A.O., D.P. Beiting, C. Tato, B. John, G. Oldenhove, C.G. Lombana, G.H. Pritchard, J.S. Silver, N.
795 Bouladoux, J.S. Stumhofer, T.H. Harris, J. Grainger, E.D. Wojno, S. Wagage, D.S. Roos, P.
796 Scott, L.A. Turka, S. Cherry, S.L. Reiner, D. Cua, Y. Belkaid, M.M. Elloso, and C.A. Hunter.
797 2012. The cytokines interleukin 27 and interferon-γ promote distinct Treg cell populations
798 required to limit infection-induced pathology. *Immunity* 37:511-523.
799 Hamano, S., K. Himeno, Y. Miyazaki, K. Ishii, A. Yamanaka, A. Takeda, M. Zhang, H. Hisaeda, T.W.
800 Mak, A. Yoshimura, and H. Yoshida. 2003. WSX-1 Is Required for Resistance to
801 Trypanosoma cruzi Infection by Regulation of Proinflammatory Cytokine Production.
802 *Immunity* 19:657-667.
803 He, H., P. Xu, X. Zhang, M. Liao, Q. Dong, T. Cong, B. Tang, X. Yang, M. Ye, Y. Chang, W. Liu, X. Wang,
804 Z. Ju, and J. Wang. 2020. Aging-induced IL27Ra signaling impairs hematopoietic stem cells.
805 *Blood* 136:183-198.
806 Ibneeva, L., S.P. Singh, A. Sinha, S.E. Eski, R. Wehner, L. Rupp, I. Kovtun, J.A. Pérez-Valencia, A.
807 Gerbaulet, S. Reinhardt, M. Wobus, M. von Bonin, J. Sancho, F. Lund, A. Dahl, M. Schmitz,
808 M. Bornhäuser, T. Chavakis, B. Wielockx, and T. Grinenko. 2024. CD38 promotes
809 hematopoietic stem cell dormancy. *PLoS Biol* 22:e3002517.
810 Im, K., S. Mareninov, M.F.P. Diaz, and W.H. Yong. 2019. An Introduction to Performing
811 Immunofluorescence Staining. *Methods Mol Biol* 1897:299-311.
812 Iwasaki, H., F. Arai, Y. Kubota, M. Dahl, and T. Suda. 2010. Endothelial protein C receptor-
813 expressing hematopoietic stem cells reside in the perisinusoidal niche in fetal liver. *Blood*
814 116:544-553.
815 John, B., T.H. Harris, E.D. Tait, E.H. Wilson, B. Gregg, L.G. Ng, P. Mrass, D.S. Roos, F. Dzierszinski,
816 W. Weninger, and C.A. Hunter. 2009. Dynamic Imaging of CD8(+) T cells and dendritic cells
817 during infection with Toxoplasma gondii. *PLoS Pathog* 5:e1000505.
818 Kaufmann, E., J. Sanz, J.L. Dunn, N. Khan, L.E. Mendonça, A. Pacis, F. Tzelepis, E. Pernet, A.
819 Dumaine, J.C. Grenier, F. Mailhot-Léonard, E. Ahmed, J. Belle, R. Besla, B. Mazer, I.L. King,
820 A. Nijnik, C.S. Robbins, L.B. Barreiro, and M. Divangahi. 2018. BCG Educates Hematopoietic
821 Stem Cells to Generate Protective Innate Immunity against Tuberculosis. *Cell* 172:176-
822 190.e119.

823 Khan, N., J. Downey, J. Sanz, E. Kaufmann, B. Blankenhaus, A. Pacis, E. Pernet, E. Ahmed, S.
824 Cardoso, A. Nijnik, B. Mazer, C. Sassetti, M.A. Behr, M.P. Soares, L.B. Barreiro, and M.
825 Divangahi. 2020. M. tuberculosis Reprograms Hematopoietic Stem Cells to Limit
826 Myelopoiesis and Impair Trained Immunity. *Cell* 183:752-770.e722.
827 Kilgore, A.M., S. Welsh, E.E. Cheney, A. Chitrakar, T.J. Blain, B.J. Kedl, C.A. Hunter, N.D. Pennock,
828 and R.M. Kedl. 2018. IL-27p28 Production by XCR1(+) Dendritic Cells and Monocytes
829 Effectively Predicts Adjuvant-Elicited CD8(+) T Cell Responses. *Immunohorizons* 2:1-11.
830 Kimura, D., M. Miyakoda, K. Kimura, K. Honma, H. Hara, H. Yoshida, and K. Yui. 2016. Interleukin-
831 27-Producing CD4(+) T Cells Regulate Protective Immunity during Malaria Parasite
832 Infection. *Immunity* 44:672-682.
833 King, K.Y., M.T. Baldridge, D.C. Weksberg, S.M. Chambers, G.L. Lukov, S. Wu, N.C. Boles, S.Y. Jung,
834 J. Qin, D. Liu, Z. Songyang, N.T. Eissa, G.A. Taylor, and M.A. Goodell. 2011. Irgm1 protects
835 hematopoietic stem cells by negative regulation of IFN signaling. *Blood* 118:1525-1533.
836 Lin, C.-H., C.-J. Wu, S. Cho, R. Patkar, W.J. Huth, L.-L. Lin, M.-C. Chen, E. Israelsson, J. Betts, M.
837 Niedzielska, S.A. Patel, H.G. Duong, R.R. Gerner, C.-Y. Hsu, M. Catley, R.A. Maciewicz, H.
838 Chu, M. Raffatellu, J.T. Chang, and L.-F. Lu. 2023. Selective IL-27 production by intestinal
839 regulatory T cells permits gut-specific regulation of TH17 cell immunity. *Nature*
840 *Immunology* 24:2108-2120.
841 Link, D.C. 2000. Mechanisms of granulocyte colony-stimulating factor-induced hematopoietic
842 progenitor-cell mobilization. *Semin Hematol* 37:25-32.
843 Liu, F.D.M., E.E. Kenngott, M.F. Schröter, A. Kühl, S. Jennrich, R. Watzlawick, U. Hoffmann, T. Wolff,
844 S. Norley, A. Scheffold, J.S. Stumhofer, C.J.M. Saris, J.M. Schwab, C.A. Hunter, G.F. Debes,
845 and A. Hamann. 2014. Timed Action of IL-27 Protects from Immunopathology while
846 Preserving Defense in Influenza. *PLOS Pathogens* 10:e1004110.
847 Liu, G., O. Abas, Y. Fu, Y. Chen, A.B. Strickland, D. Sun, and M. Shi. 2021. IL-27 Negatively Regulates
848 Tip-DC Development during Infection. *mBio* 12:
849 Liu, Y., Y. Chen, X. Deng, and J. Zhou. 2020. ATF3 Prevents Stress-Induced Hematopoietic Stem Cell
850 Exhaustion. *Front Cell Dev Biol* 8:585771.
851 Ma, Z., J. Xu, L. Wu, J. Wang, Q. Lin, F.A. Chowdhury, M.H.H. Mazumder, G. Hu, X. Li, and W. Du.
852 2020. Hes1 deficiency causes hematopoietic stem cell exhaustion. *Stem Cells* 38:756-768.
853 MacNamara, K.C., M. Jones, O. Martin, and G.M. Winslow. 2011a. Transient activation of
854 hematopoietic stem and progenitor cells by IFNγ during acute bacterial infection. *PLoS*
855 *One* 6:e28669.
856 MacNamara, K.C., K. Oduro, O. Martin, D.D. Jones, M. McLaughlin, K. Choi, D.L. Borjesson, and
857 G.M. Winslow. 2011b. Infection-induced myelopoiesis during intracellular bacterial
858 infection is critically dependent upon IFN-γ signaling. *J Immunol* 186:1032-1043.
859 Maeda, K., Y. Baba, Y. Nagai, K. Miyazaki, A. Malykhin, K. Nakamura, P.W. Kincade, N. Sakaguchi,
860 and K.M. Coggeshall. 2005. IL-6 blocks a discrete early step in lymphopoiesis. *Blood*
861 106:879-885.
862 Matatall, K.A., C.C. Shen, G.A. Challen, and K.Y. King. 2014. Type II interferon promotes
863 differentiation of myeloid-biased hematopoietic stem cells. *Stem Cells* 32:3023-3030.
864 McCabe, A., Y. Zhang, V. Thai, M. Jones, M.B. Jordan, and K.C. MacNamara. 2015. Macrophage-
865 Lineage Cells Negatively Regulate the Hematopoietic Stem Cell Pool in Response to
866 Interferon Gamma at Steady State and During Infection. *Stem Cells* 33:2294-2305.

867 Miner, X., Z. Shanshan, D. Fang, Z. Qingyun, W. Jinhong, W. Chenchen, Z. Caiying, Z. Sen, L.
868 Bingqing, W. Peng, and E. Hideo. 2021. Granulocyte colony-stimulating factor directly acts
869 on mouse lymphoid-biased but not myeloid-biased hematopoietic stem cells.
870 *Haematologica* 106:1647-1658.
871 Mirantes, C., E. Passegué, and E.M. Pietras. 2014. Pro-inflammatory cytokines: emerging players
872 regulating HSC function in normal and diseased hematopoiesis. *Exp Cell Res* 329:248-254.
873 Morales-Mantilla, D.E., B. Kain, D. Le, A.R. Flores, S. Paust, and K.Y. King. 2022. Hematopoietic
874 stem and progenitor cells improve survival from sepsis by boosting immunomodulatory
875 cells. *eLife* 11:e74561.
876 Ochando, J., W.J.M. Mulder, J.C. Madsen, M.G. Netea, and R. Duivenvoorden. 2023. Trained
877 immunity — basic concepts and contributions to immunopathology. *Nature Reviews*
878 *Nephrology* 19:23-37.
879 Pardy, R.D., K.A. Walzer, B.A. Wallbank, J.H. Byerly, K.M. O'Dea, I.S. Cohn, B.E. Haskins, J.L.
880 Roncaioli, E.J. Smith, G.Y. Buenconsejo, B. Striepen, and C.A. Hunter. 2024. Analysis of
881 intestinal epithelial cell responses to Cryptosporidium highlights the temporal effects of
882 IFN-γ on parasite restriction. *PLOS Pathogens* 20:e1011820.
883 Parmar, K., P. Mauch, J.A. Vergilio, R. Sackstein, and J.D. Down. 2007. Distribution of
884 hematopoietic stem cells in the bone marrow according to regional hypoxia. *Proc Natl*
885 *Acad Sci U S A* 104:5431-5436.
886 Peshkova, I.O., T. Aghayev, A.R. Fatkhullina, P. Makhov, E.K. Titerina, S. Eguchi, Y.F. Tan, A.V.
887 Kossenkov, M.V. Khoreva, L.V. Gankovskaya, S.M. Sykes, and E.K. Koltsova. 2019. IL-27
888 receptor-regulated stress myelopoiesis drives abdominal aortic aneurysm development.
889 *Nature Communications* 10:5046.
890 Pflanz, S., L. Hibbert, J. Mattson, R. Rosales, E. Vaisberg, J.F. Bazan, J.H. Phillips, T.K. McClanahan,
891 R. de Waal Malefyt, and R.A. Kastelein. 2004. WSX-1 and Glycoprotein 130 Constitute a
892 Signal-Transducing Receptor for IL-27. *The Journal of Immunology* 172:2225-2231.
893 Pflanz, S., J.C. Timans, J. Cheung, R. Rosales, H. Kanzler, J. Gilbert, L. Hibbert, T. Churakova, M.
894 Travis, E. Vaisberg, W.M. Blumenschein, J.D. Mattson, J.L. Wagner, W. To, S. Zurawski, T.K.
895 McClanahan, D.M. Gorman, J.F. Bazan, R. de Waal Malefyt, D. Rennick, and R.A. Kastelein.
896 2002. IL-27, a Heterodimeric Cytokine Composed of EBI3 and p28 Protein, Induces
897 Proliferation of Naive CD4+ T Cells. *Immunity* 16:779-790.
898 Pietras, E.M., R. Lakshminarasimhan, J.M. Techner, S. Fong, J. Flach, M. Binnewies, and E.
899 Passegué. 2014. Re-entry into quiescence protects hematopoietic stem cells from the
900 killing effect of chronic exposure to type I interferons. *J Exp Med* 211:245-262.
901 Revuelta, M., and A. Matheu. 2017. Autophagy in stem cell aging. *Aging Cell* 16:912-915.
902 Reynaud, D., E. Pietras, K. Barry-Holson, A. Mir, M. Binnewies, M. Jeanne, O. Sala-Torra, J.P. Radich,
903 and E. Passegué. 2011. IL-6 controls leukemic multipotent progenitor cell fate and
904 contributes to chronic myelogenous leukemia development. *Cancer Cell* 20:661-673.
905 Ross, J.B., L.M. Myers, J.J. Noh, M.M. Collins, A.B. Carmody, R.J. Messer, E. Dhuey, K.J. Hasenkrug,
906 and I.L. Weissman. 2024. Depleting myeloid-biased haematopoietic stem cells rejuvenates
907 aged immunity. *Nature* 628:162-170.
908 Samusik, N., Z. Good, M.H. Spitzer, K.L. Davis, and G.P. Nolan. 2016. Automated mapping of
909 phenotype space with single-cell data. *Nat Methods* 13:493-496.

Säwen, P., M. Eldeeb, E. Erlandsson, T.A. Kristiansen, C. Laterza, Z. Kokaia, G. Karlsson, J. Yuan, S. Soneji, P.K. Mandal, D.J. Rossi, and D. Bryder. 2018. Murine HSCs contribute actively to native hematopoiesis but with reduced differentiation capacity upon aging. *eLife* 7:e41258.

Schindelin, J., I. Arganda-Carreras, E. Frise, V. Kaynig, M. Longair, T. Pietzsch, S. Preibisch, C. Rueden, S. Saalfeld, B. Schmid, J.-Y. Tinevez, D.J. White, V. Hartenstein, K. Eliceiri, P. Tomancak, and A. Cardona. 2012. Fiji: an open-source platform for biological-image analysis. *Nature Methods* 9:676-682.

Seita, J., M. Asakawa, J. Ooehara, S. Takayanagi, Y. Morita, N. Watanabe, K. Fujita, M. Kudo, J. Mizuguchi, H. Ema, H. Nakauchi, and T. Yoshimoto. 2008. Interleukin-27 directly induces differentiation in hematopoietic stem cells. *Blood* 111:1903-1912.

Seyfried, A.N., J.M. Maloney, and K.C. MacNamara. 2020. Macrophages Orchestrate Hematopoietic Programs and Regulate HSC Function During Inflammatory Stress. *Front Immunol* 11:1499.

Siminovitch, L., J.E. Till, and E.A. McCulloch. 1964. Decline in colony-forming ability of marrow cells subjected to serial transplantation into irradiated mice. *Journal of Cellular and Comparative Physiology* 64:23-31.

Singh, S., B. Jakubison, and J.R. Keller. 2020. Protection of hematopoietic stem cells from stress-induced exhaustion and aging. *Curr Opin Hematol* 27:225-231.

Singh, S.K., S. Singh, S. Gadomski, L. Sun, A. Pfannenstein, V. Magidson, X. Chen, S. Kozlov, L. Tessarollo, K.D. Klarmann, and J.R. Keller. 2018. Id1 Ablation Protects Hematopoietic Stem Cells from Stress-Induced Exhaustion and Aging. *Cell Stem Cell* 23:252-265.e258.

Stifter, S.A., N. Bhattacharyya, A.J. Sawyer, T.A. Cootes, J. Stambas, S.E. Doyle, L. Feigenbaum, W.E. Paul, W.J. Britton, A. Sher, and C.G. Feng. 2019. Visualizing the Selectivity and Dynamics of Interferon Signaling In Vivo. *Cell Rep* 29:3539-3550.e3534.

Sun, D., M. Zhang, and M. Shi. 2017. IL-27 limits neutrophil mediated pathology during pulmonary infection with Cryptococcus neoformans. *The Journal of Immunology* 198:123.128-123.128.

Villarino, A., L. Hibbert, L. Lieberman, E. Wilson, T. Mak, H. Yoshida, R.A. Kastelein, C. Saris, and C.A. Hunter. 2003. The IL-27R (WSX-1) is required to suppress T cell hyperactivity during infection. *Immunity* 19:645-655.

Weissman, I.L. 2000. Stem Cells: Units of Development, Units of Regeneration, and Units in Evolution. *Cell* 100:157-168.

Wirtz , S., I. Tubbe , P.R. Galle , H.J. Schild , M. Birkenbach , R.S. Blumberg , and M.F. Neurath 2006. Protection from lethal septic peritonitis by neutralizing the biological function of interleukin 27. *Journal of Experimental Medicine* 203:1875-1881.

Zhao, H.G., and M. Deininger. 2023. Always stressed but never exhausted: how stem cells in myeloid neoplasms avoid extinction in inflammatory conditions. *Blood* 141:2797-2812.

Zhu, J., J. Yu, A. Hu, J.Q. Liu, X. Pan, G. Xin, W.E. Carson, Z. Li, Y. Yang, and X.F. Bai. 2023. IL-27 Gene Therapy Induces Stat3-Mediated Expansion of CD11b+Gr1+ Myeloid Cells and Promotes Accumulation of M1 Macrophages in the Tumor Microenvironment. *J Immunol* 211:895-902.

Figure 1

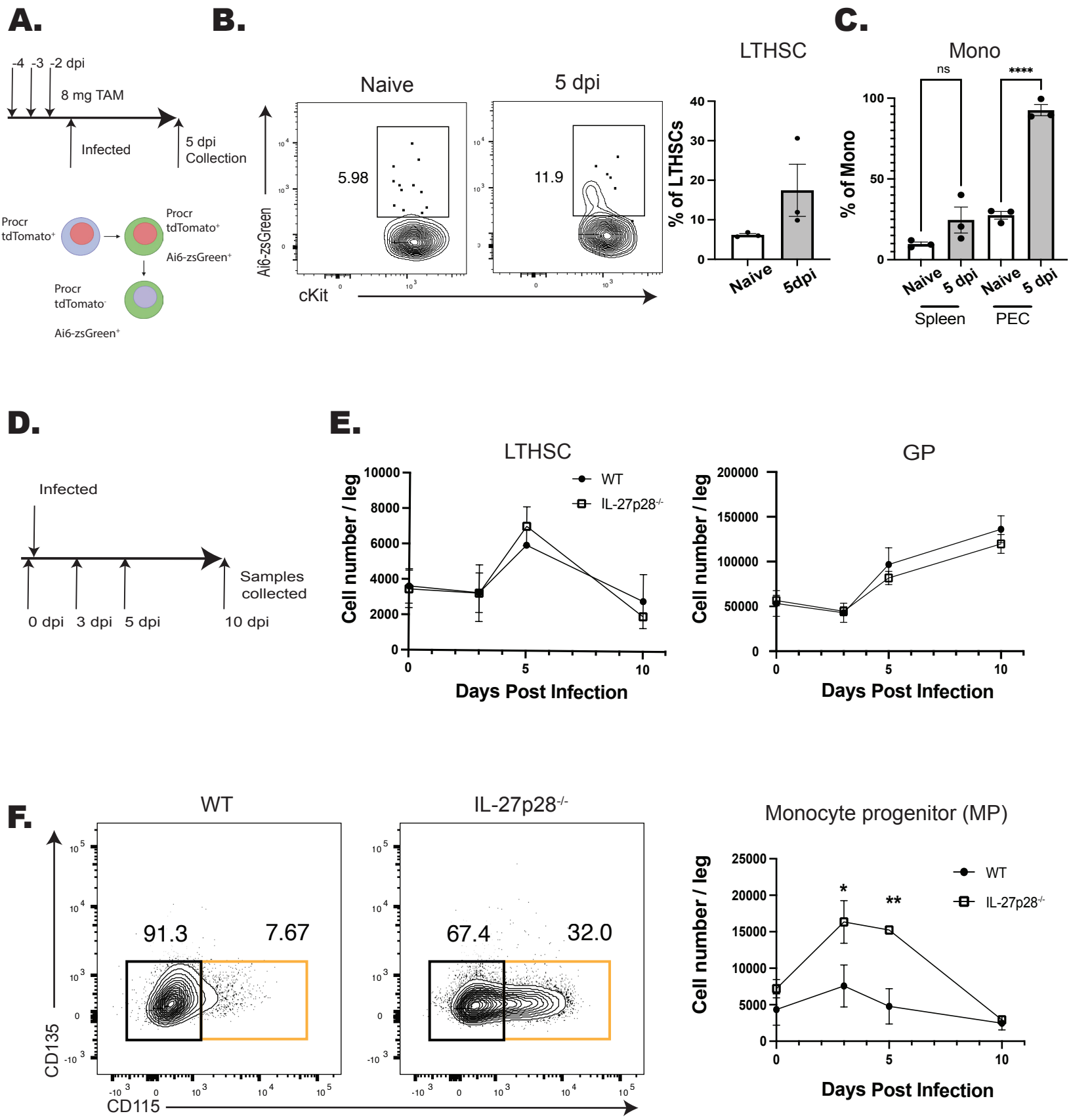
A.
-4 -3 -2 dpi
8 mg TAM
Infected
5 dpi Collection
Procr tdTomato+
Procr tdTomato+
Ai6-zsGreen+
Procr tdTomato-
Ai6-zsGreen+
B.
Naive
5 dpi
5.98
11.9
Ai6-zsGreen
cKit
LTHSC
% of LTHSCs
Naive
5dpi
C.
Mono
ns
****
% of Mono
Naive
5 dpi
Naive
5 dpi
Spleen
PEC
D.
Infected
Samples collected
0 dpi
3 dpi
5 dpi
10 dpi
E.
LTHSC
GP
WT
IL-27p28-/-
Cell number / leg
Days Post Infection
F.
WT
IL-27p28-/-
91.3
7.67
67.4
32.0
CD135
CD115
Monocyte progenitor (MP)
Cell number / leg
Days Post Infection
WT
IL-27p28-/-
*
**

Supplemental Figure 1

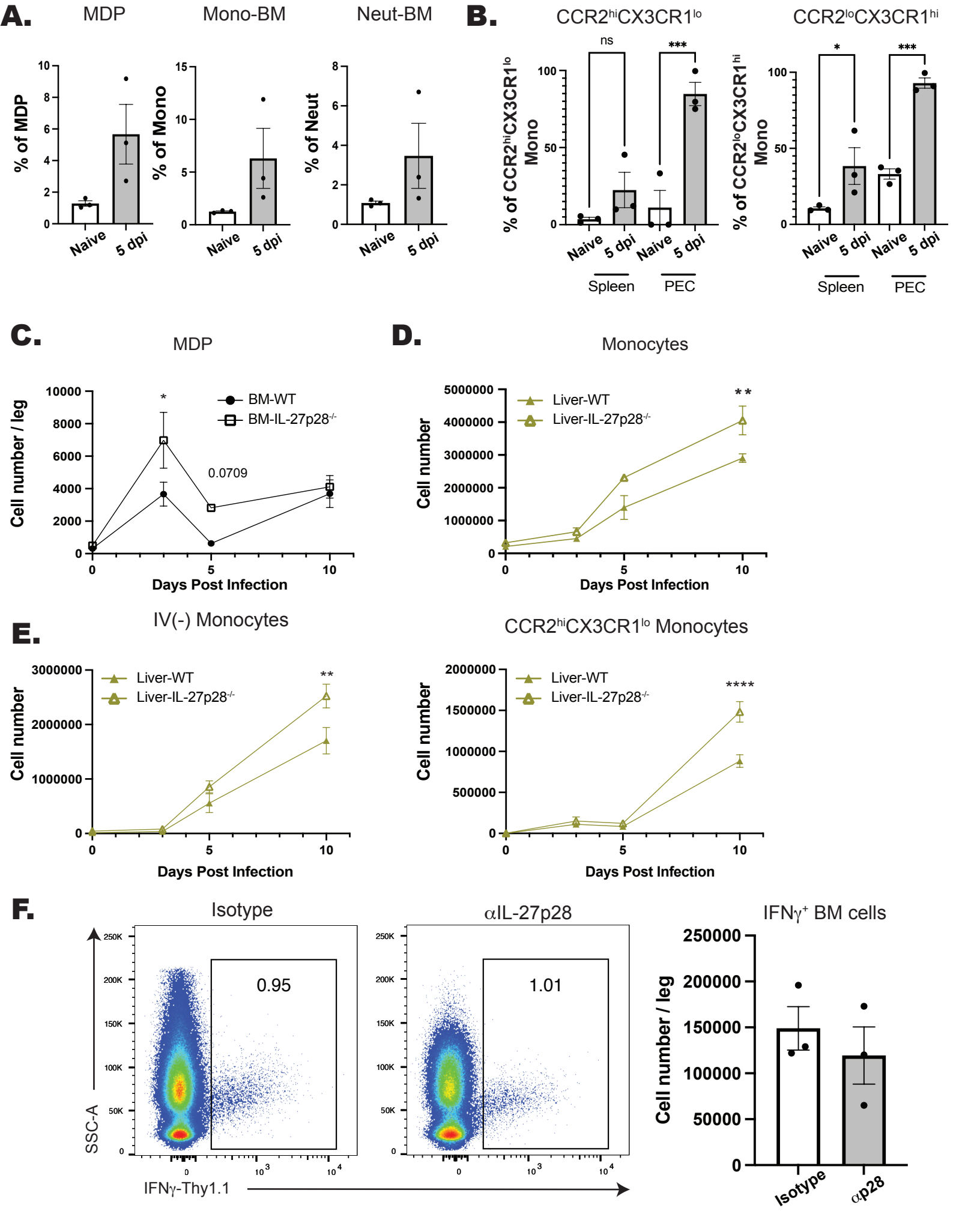

Supplemental Figure 2

Bone marrow gating strategy

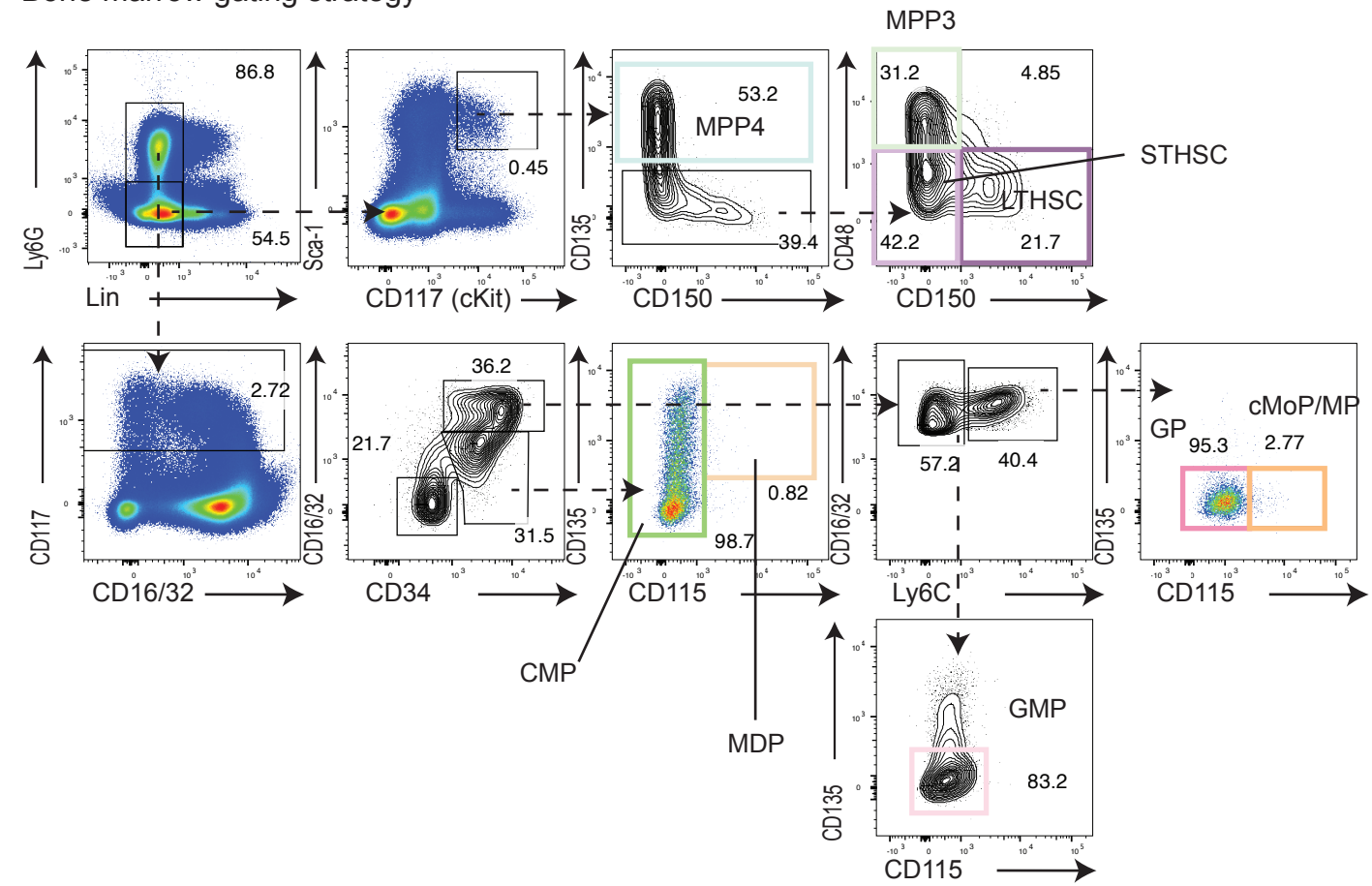

Periphery gating strategy

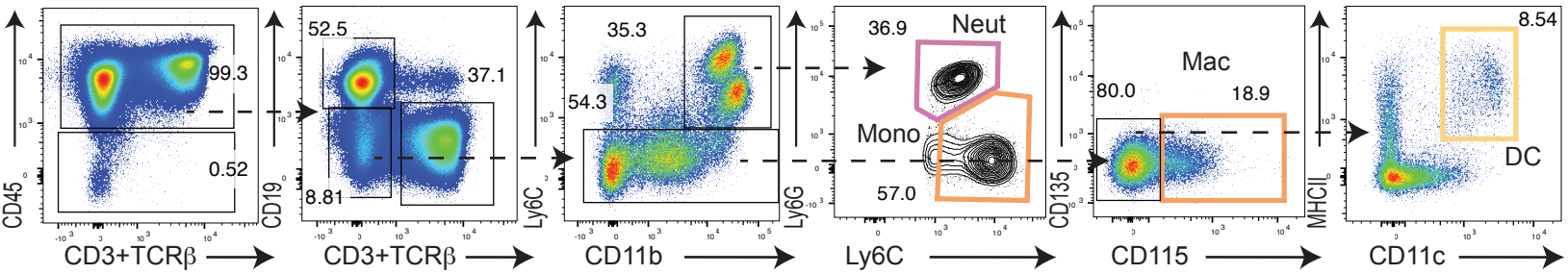

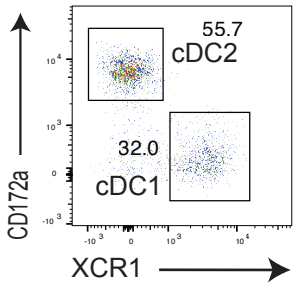

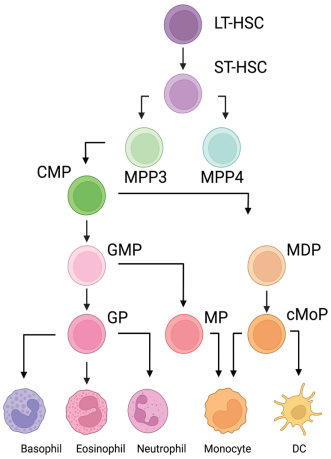

Bone marrow surface markers

Cell Type	Defining Surface Markers
Long-Term Hematopoietic Stem Cell (LTHSC)	Lin (CD3, B220, NK1.1, Ly6G)$^-$, Sca-1$^+$, CD117$^+$, CD135$^-$, CD48$^-$, CD150$^+$
Short-Term Hematopoietic Stem Cell (STHSC)	Lin (CD3, B220, NK1.1, Ly6G)$^-$, Sca-1$^+$, CD117$^+$, CD135$^-$, CD48$^-$, CD150$^-$
Multi-Potent Progenitor 3 (MPP3)	Lin (CD3, B220, NK1.1, Ly6G)$^-$, Sca-1$^+$, CD117$^+$, CD135$^-$, CD48$^+$, CD150$^-$
Multi-Potent Progenitor 4 (MPP4)	Lin (CD3, B220, NK1.1, Ly6G)$^-$, Sca-1$^+$, CD117$^+$, CD135$^+$
Common Myeloid Progenitor (CMP)	(CD3, B220, NK1.1)$^-$, CD117$^+$, CD34$^+$, CD16/32^{lo}, CD115$^-$
Monocyte-Dendritic cell Progenitor (MDP)	(CD3, B220, NK1.1)$^-$, CD117$^+$, CD34$^+$, CD16/32^{lo}, CD115$^+$
Common Monocyte Progenitor (cMoP)/ Monocyte Progenitor (MP)	(CD3, B220, NK1.1)$^-$, CD117$^+$, CD34$^+$, CD16/32^{hi}, Ly6C$^+$, CD135$^-$, CD115$^+$
Granulocyte-Monocyte Progenitor (GMP)	(CD3, B220, NK1.1)$^-$, CD117$^+$, CD34$^+$, CD16/32^{hi}, Ly6C$^-$, CD135$^-$, CD115$^-$
Granulocyte Progenitor (GP)	(CD3, B220, NK1.1)$^-$, CD117$^+$, CD34$^+$, CD16/32^{hi}, Ly6C$^+$, CD135$^-$, CD115$^-$

Periphery surface markers

Cell Type	Defining Surface Markers
T cells	CD45$^+$, CD19$^-$, CD3$^+$, TCRβ$^+$
B cells	CD45$^+$, CD19$^+$, CD3$^-$, TCRβ$^-$
Neutrophils	CD45$^+$, CD19$^-$, CD3$^-$, TCRβ$^-$, CD11b$^+$, Ly6C$^+$, Ly6G$^+$
Monocytes	CD45$^+$, CD19$^-$, CD3$^-$, TCRβ$^-$, CD11b$^+$, Ly6C$^+$, Ly6G$^-$
Macrophages	CD45$^+$, CD19$^-$, CD3$^-$, TCRβ$^-$, Ly6C$^-$, Ly6G$^-$, CD64$^+$
Dendritic Cells	CD45$^+$, CD19$^-$, CD3$^-$, TCRβ$^-$, Ly6C$^-$, Ly6G$^-$, CD64$^-$, CD11c$^+$, MHCII$^+$
Classical Dendritic Cells 1	CD45$^+$, CD19$^-$, CD3$^-$, TCRβ$^-$, Ly6C$^-$, Ly6G$^-$, CD64$^-$, CD11c$^+$, MHCII$^+$, XCR1$^+$, CD172a$^-$
Classical Dendritic Cells 2	CD45$^+$, CD19$^-$, CD3$^-$, TCRβ$^-$, Ly6C$^-$, Ly6G$^-$, CD64$^-$, CD11c$^+$, MHCII$^+$, XCR1$^+$, CD172a$^-$

Figure 2

A.

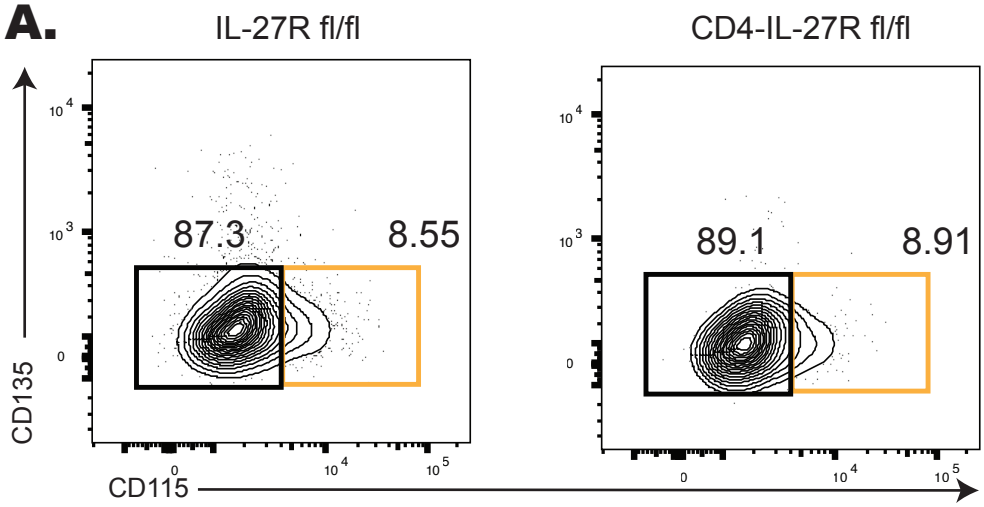

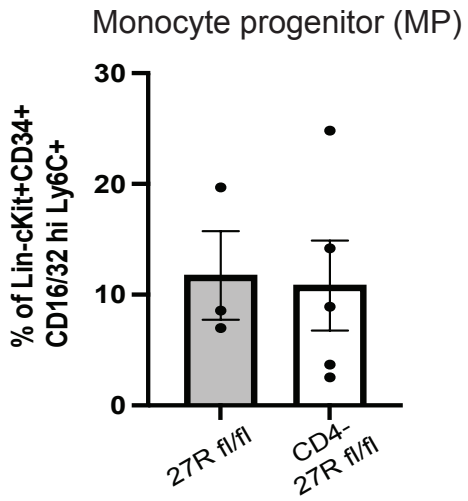

B.

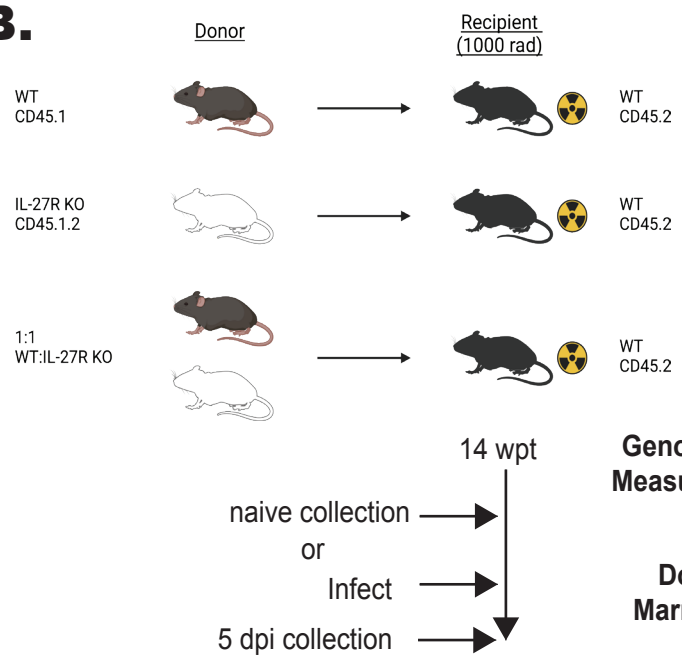

C.

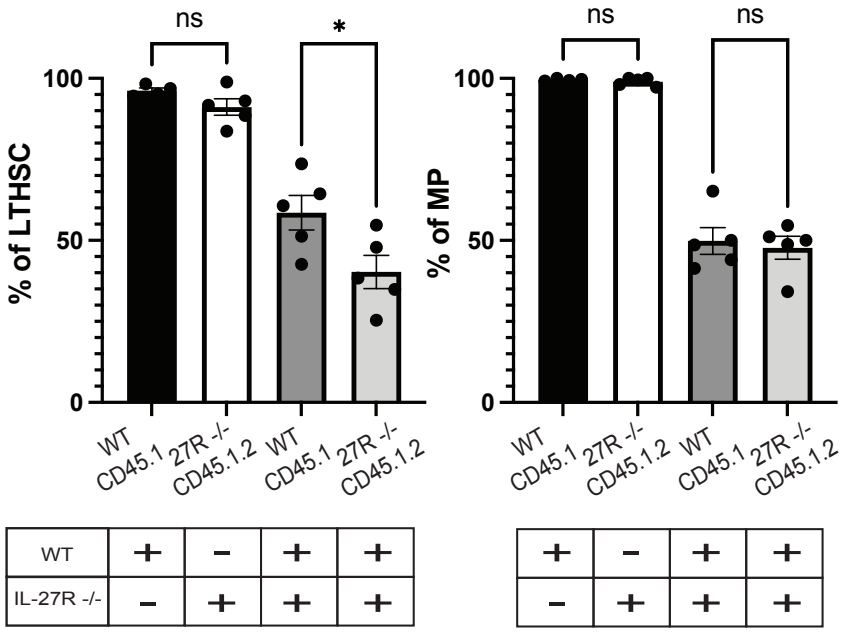

D.

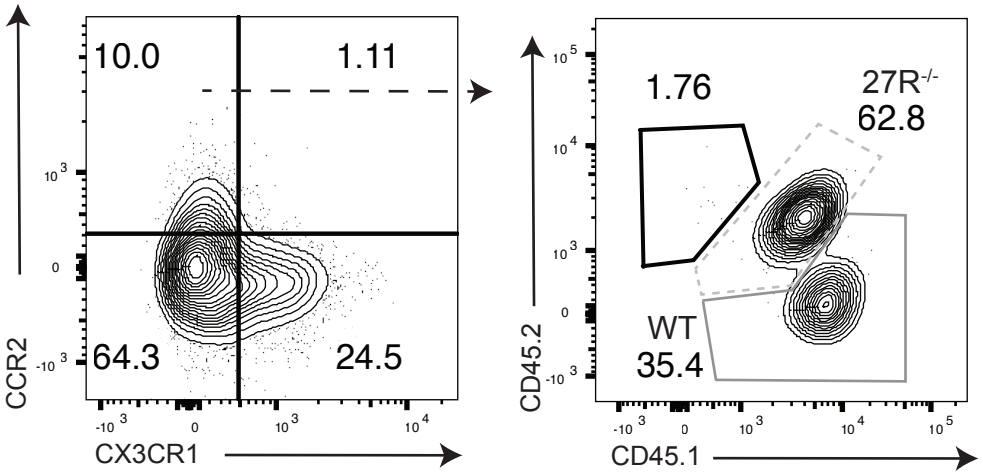

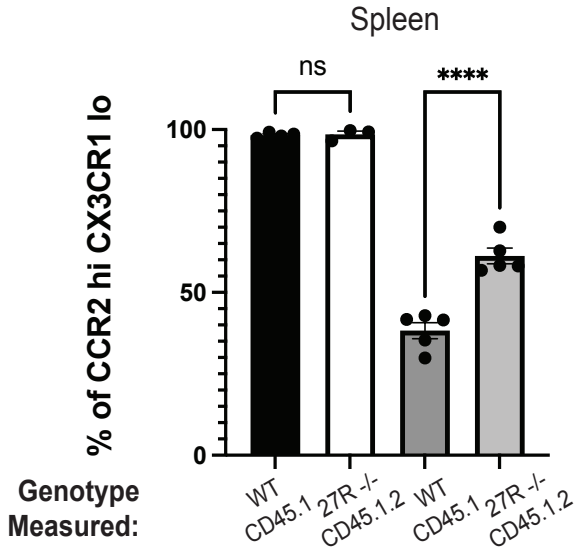

Supplemental Figure 3

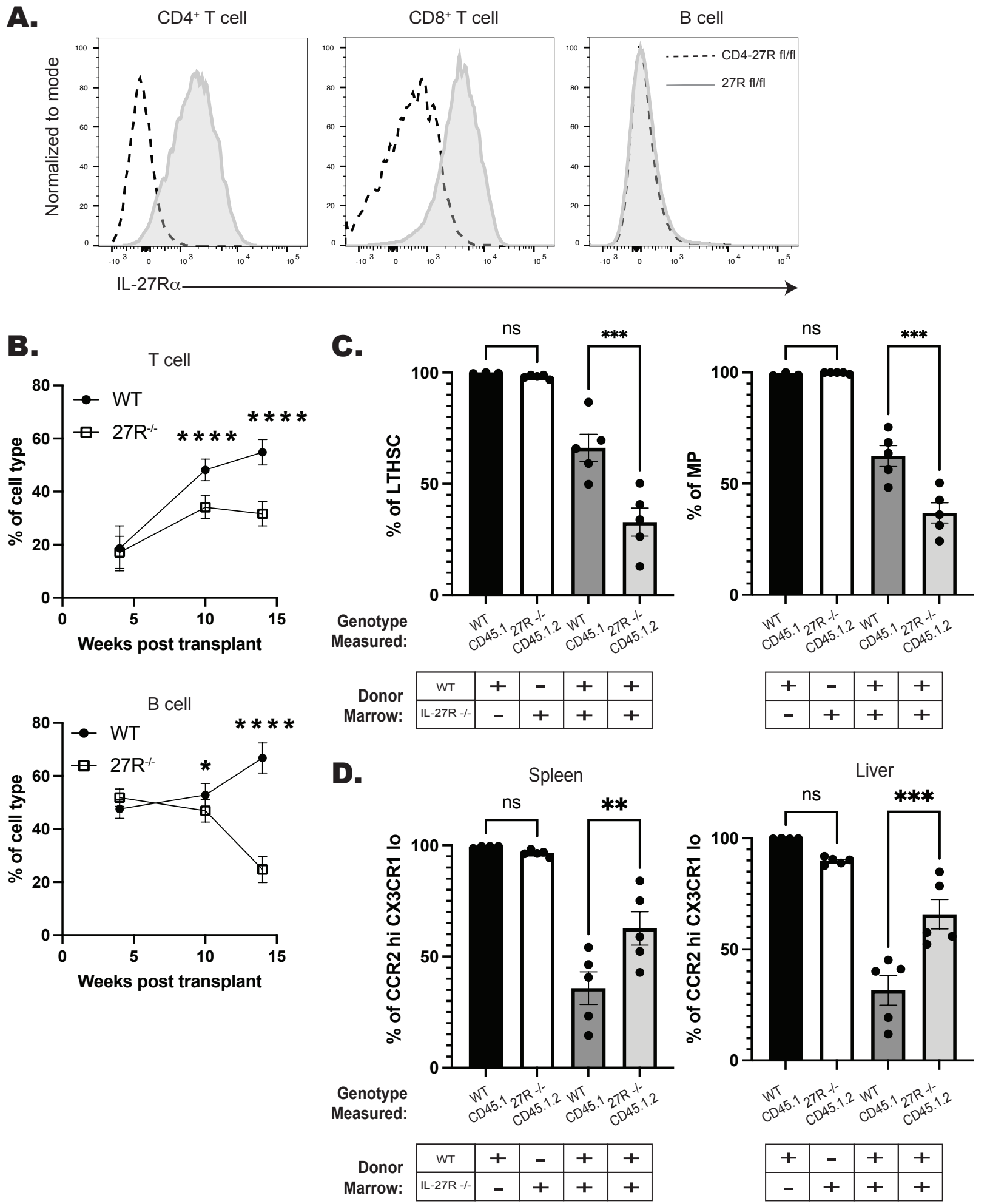

Figure 3

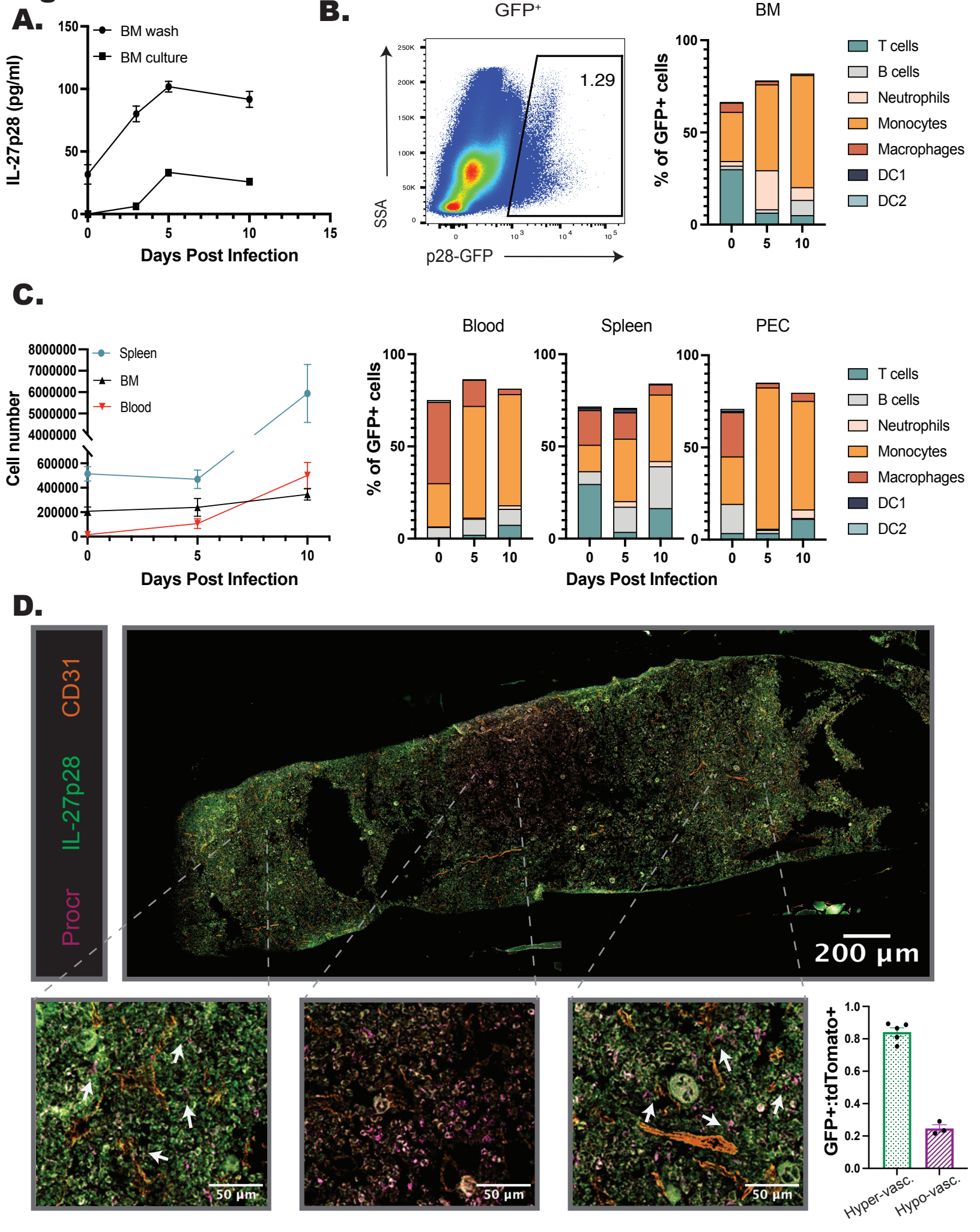
A.
BM wash
BM culture
IL-27p28 (pg/ml)
Days Post Infection
B.
GFP+
BM
1.29
SSA
p28-GFP
% of GFP+ cells
T cells
B cells
Neutrophils
Monocytes
Macrophages
DC1
DC2
C.
Spleen
BM
Blood
Cell number
Days Post Infection
Blood
Spleen
PEC
% of GFP+ cells
Days Post Infection
D.
Procr
IL-27p28
CD31
200 µm
50 µm
50 µm
50 µm
GFP+:tdTomato+
Hyper-vasc.
Hypo-vasc.

Supplemental Figure 4

A.

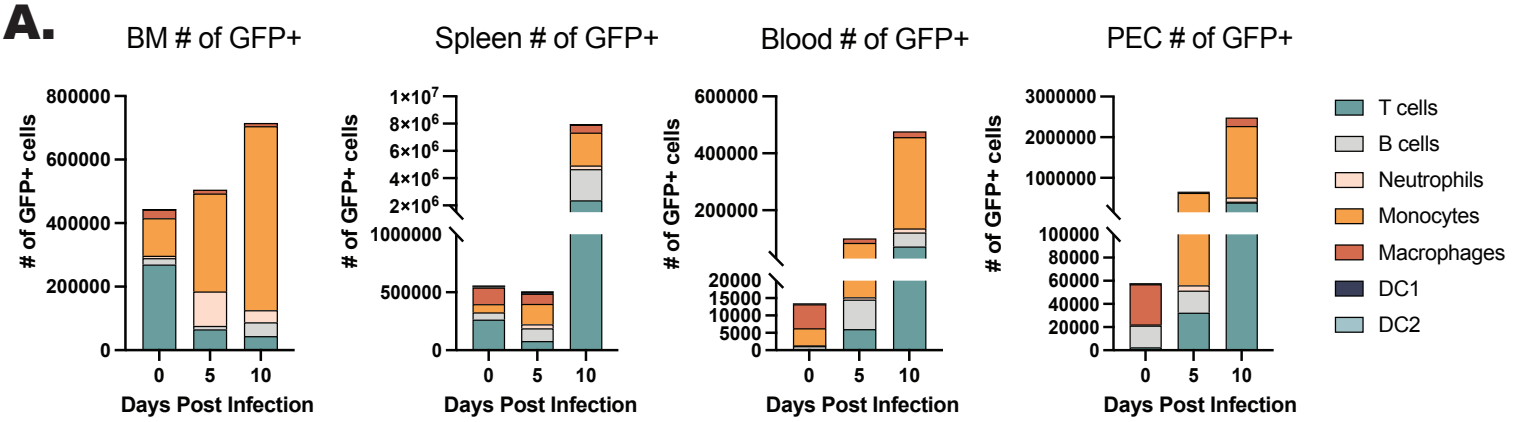

B.

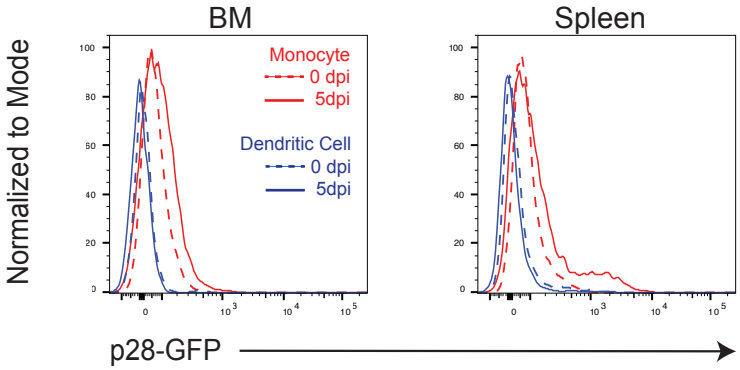

C.

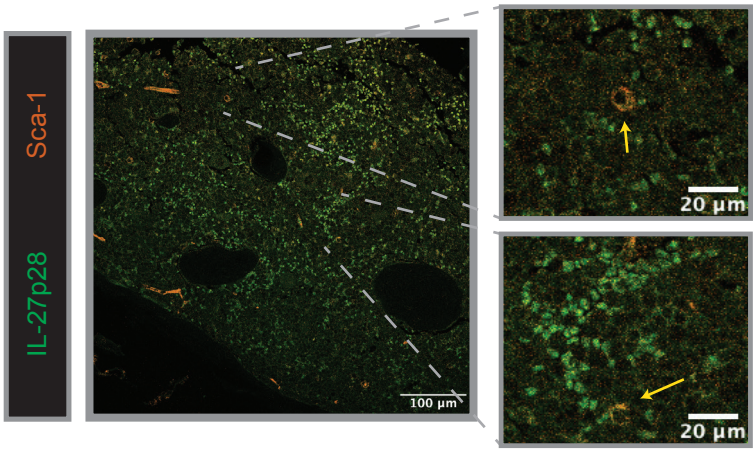

D.

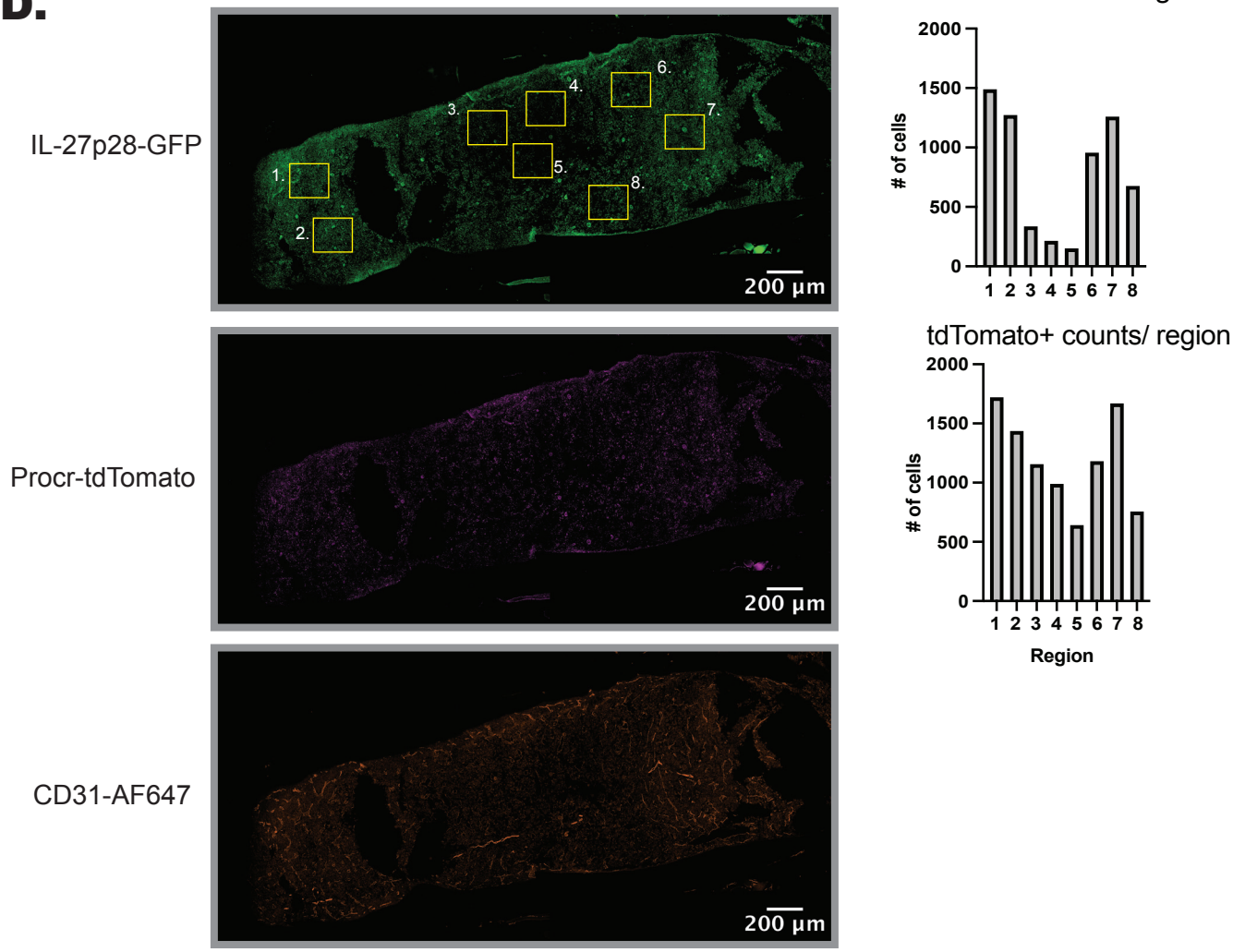

Figure 4

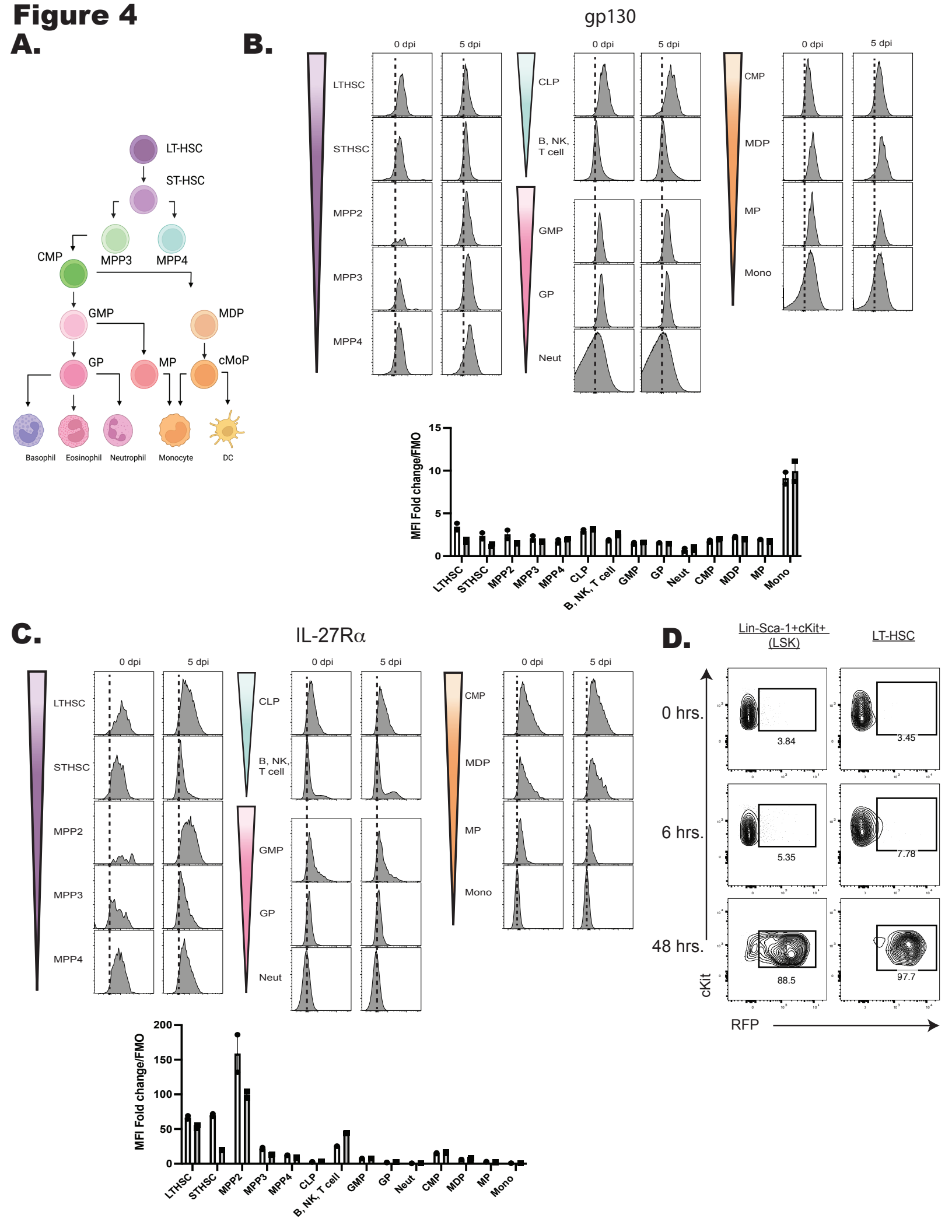
A.
LT-HSC
ST-HSC
MPP3
MPP4
CMP
GMP
MDP
GP
MP
cMoP
Basophil
Eosinophil
Neutrophil
Monocyte
DC
B.
gp130
0 dpi
5 dpi
LTHSC
STHSC
MPP2
MPP3
MPP4
CLP
B, NK, T cell
GMP
GP
Neut
CMP
MDP
MP
Mono
MFI Fold change/FMO
C.
IL-27Rα
D.
Lin-Sca-1+cKit+ (LSK)
LT-HSC
0 hrs.
6 hrs.
48 hrs.
3.84
3.45
5.35
7.78
88.5
97.7
cKit
RFP

Supplemental Figure 5

A.

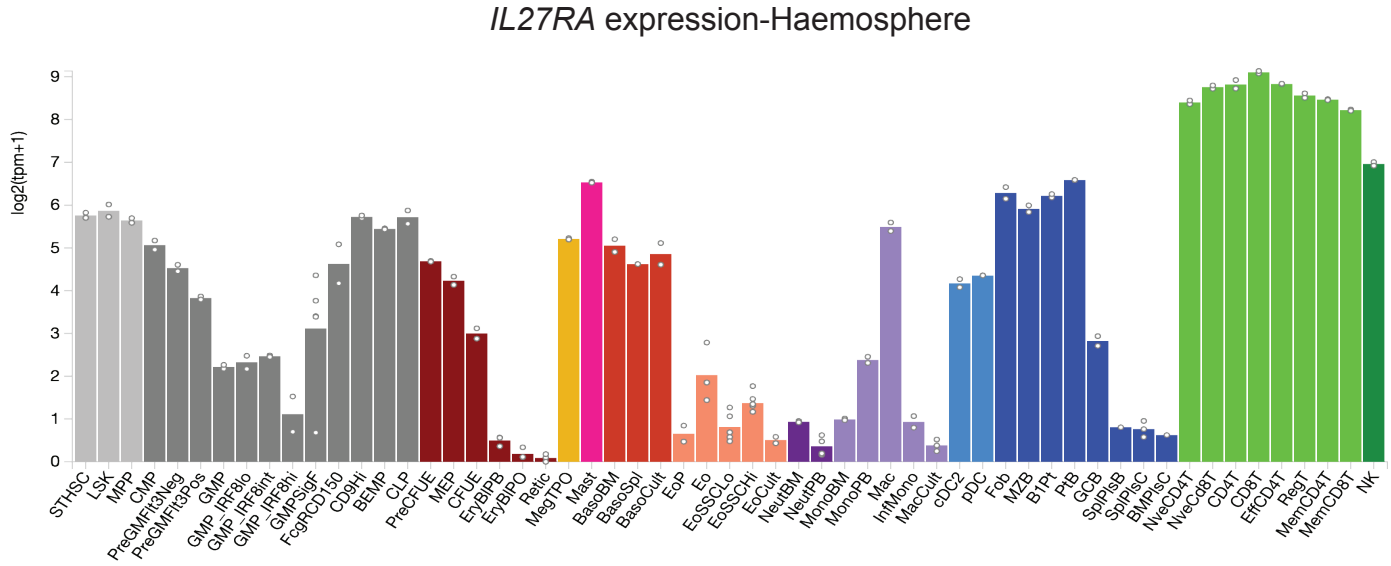

B.

C.

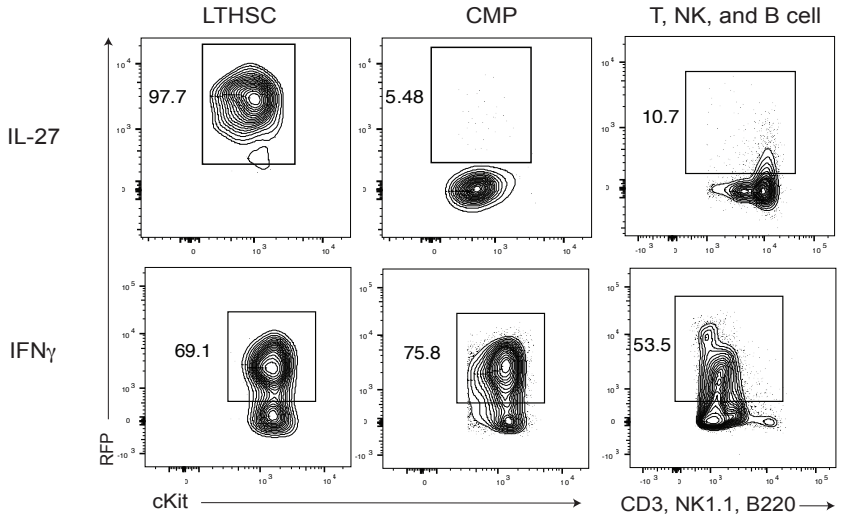

Figure 5

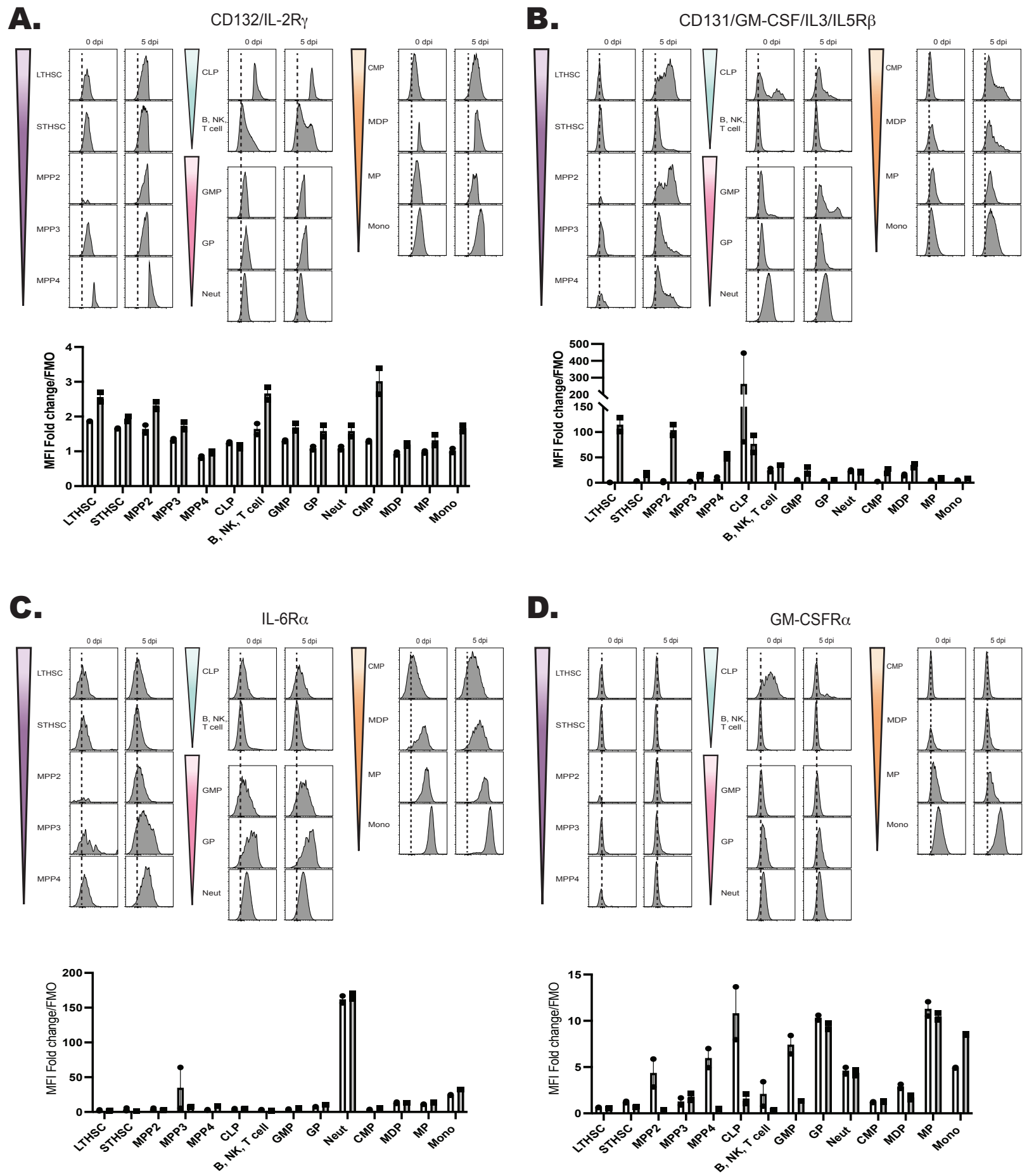
A.
CD132/IL-2Rγ
B.
CD131/GM-CSF/IL3/IL5Rβ
C.
IL-6Rα
D.
GM-CSFRα
0 dpi
5 dpi
LTHSC
STHSC
MPP2
MPP3
MPP4
CLP
B, NK, T cell
GMP
GP
Neut
CMP
MDP
MP
Mono
MFI Fold change/FMO

Supplemental Figure 6

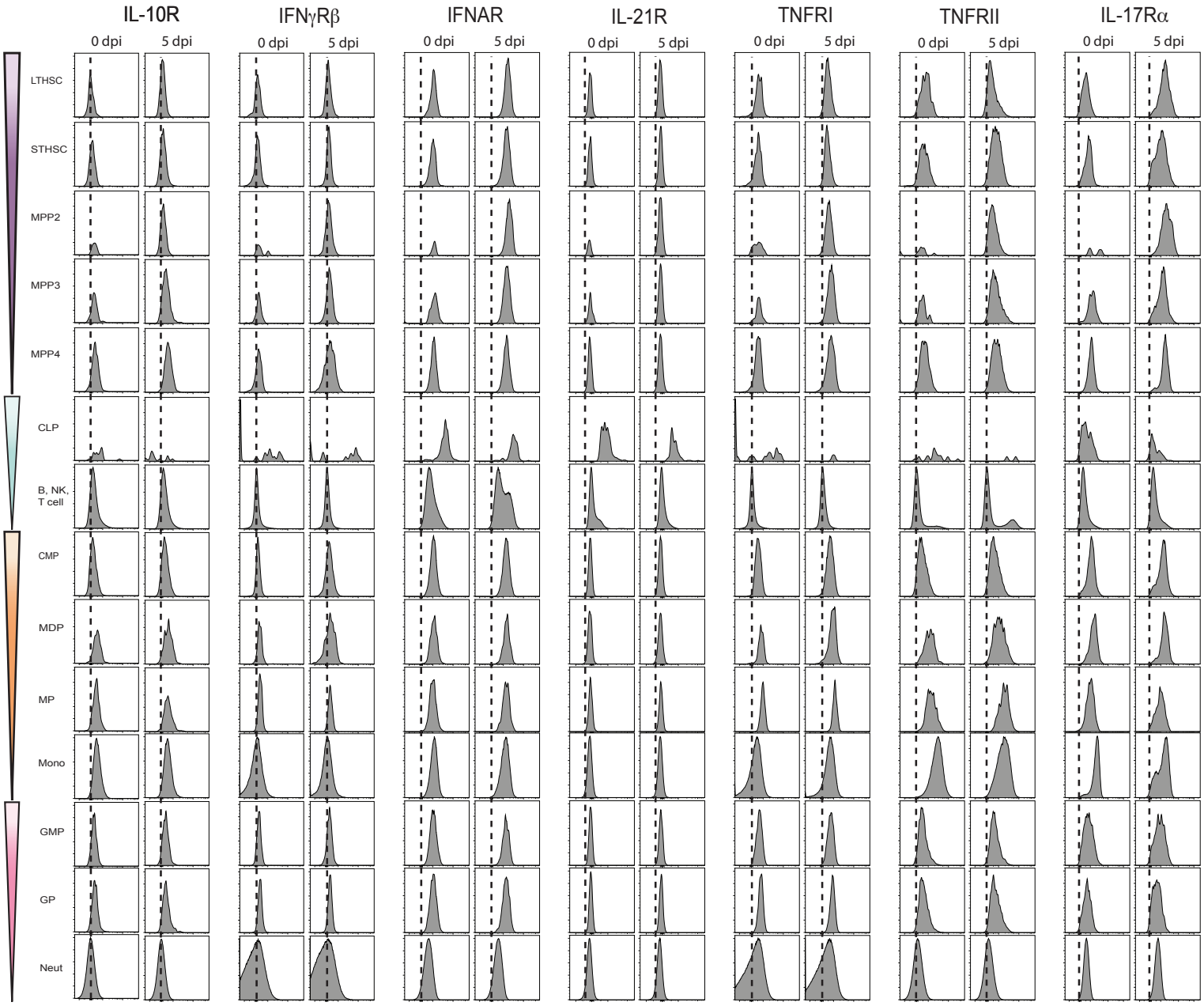

Figure 6

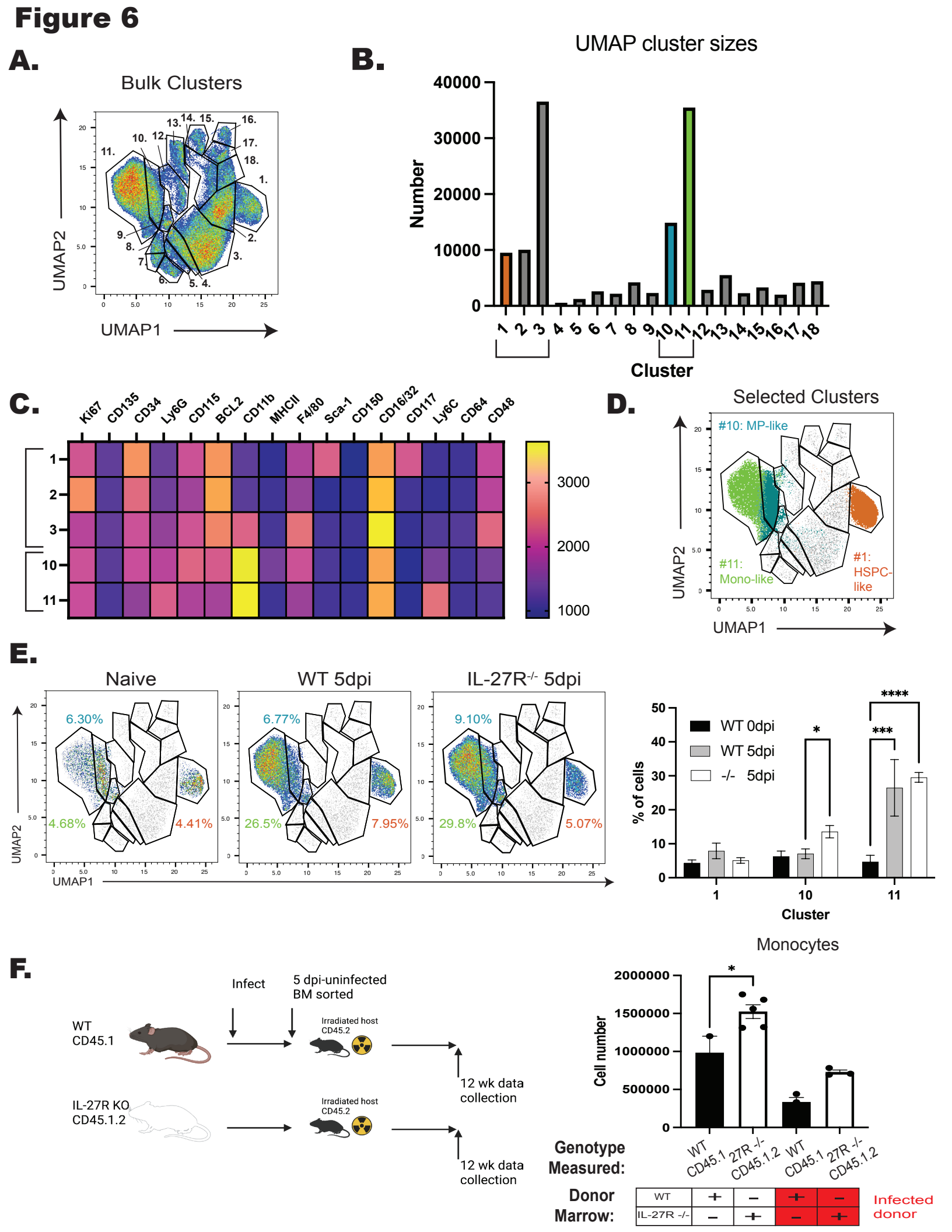
A.
Bulk Clusters
UMAP2
UMAP1
B.
UMAP cluster sizes
Number
Cluster
C.
Ki67
CD135
CD34
Ly6G
CD115
BCL2
CD11b
MHCII
F4/80
Sca-1
CD150
CD16/32
CD117
Ly6C
CD64
CD48
D.
Selected Clusters
#10: MP-like
#11: Mono-like
#1: HSPC-like
UMAP2
UMAP1
E.
Naive
WT 5dpi
IL-27R-/- 5dpi
6.30%
4.68%
4.41%
6.77%
26.5%
7.95%
9.10%
29.8%
5.07%
UMAP2
UMAP1
WT 0dpi
WT 5dpi
-/- 5dpi
% of cells
Cluster
F.
Infect
5 dpi-uninfected BM sorted
WT CD45.1
IL-27R KO CD45.1.2
Irradiated host CD45.2
12 wk data collection
Monocytes
Cell number
Genotype Measured:
WT CD45.1
27R -/- CD45.1.2
Donor Marrow:
WT
IL-27R -/-
Infected donor

Supplemental Figure 7

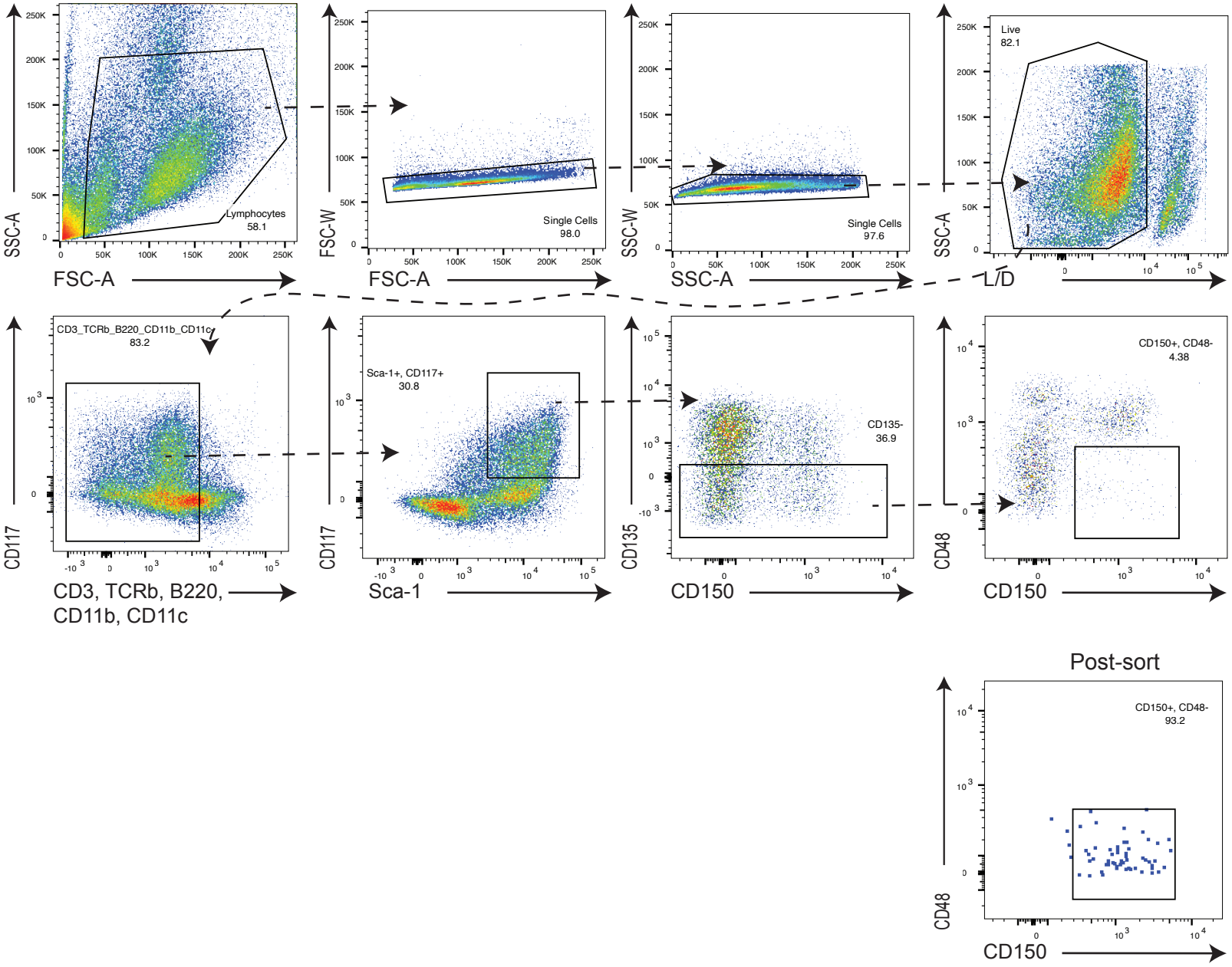

Supplemental Figure 8

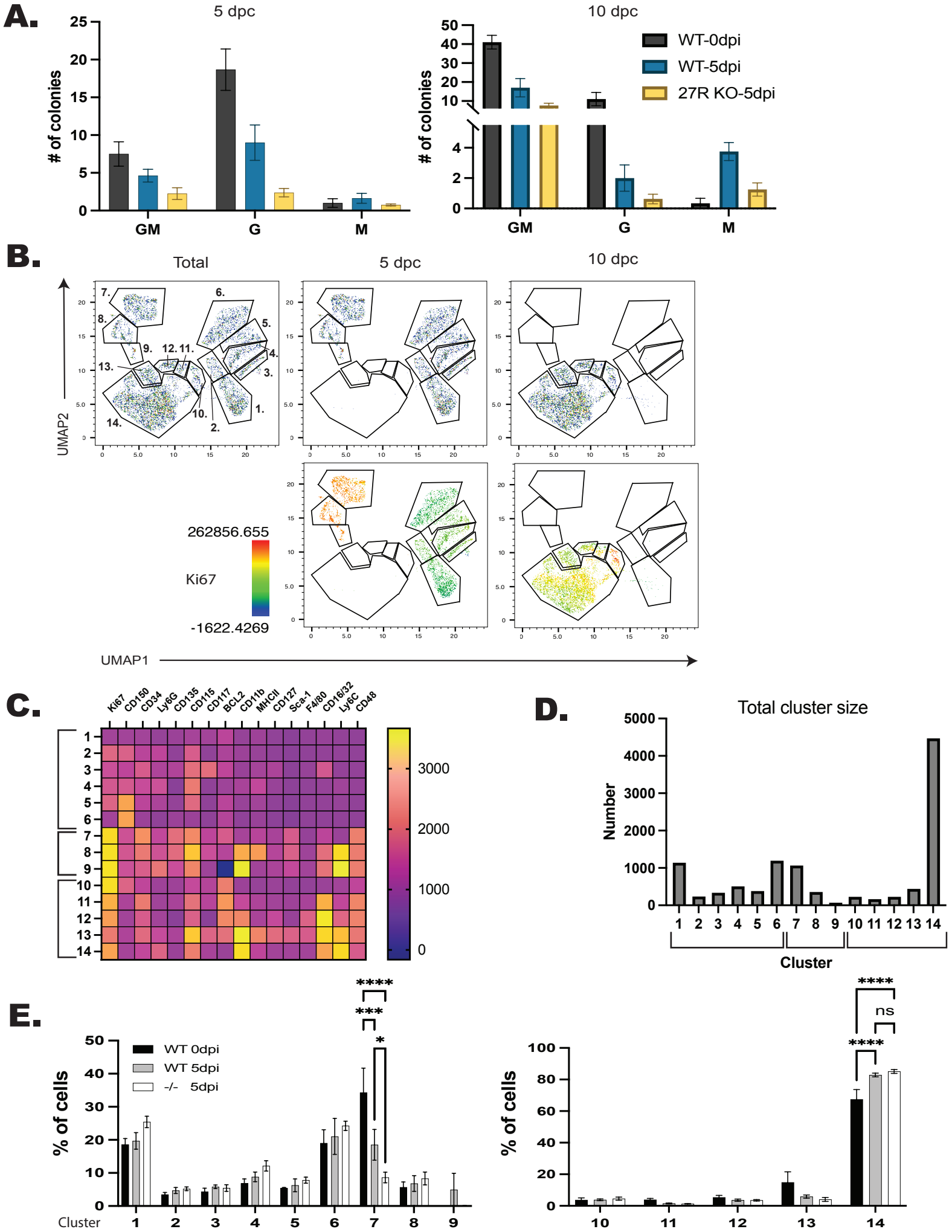

Figure 7

A.

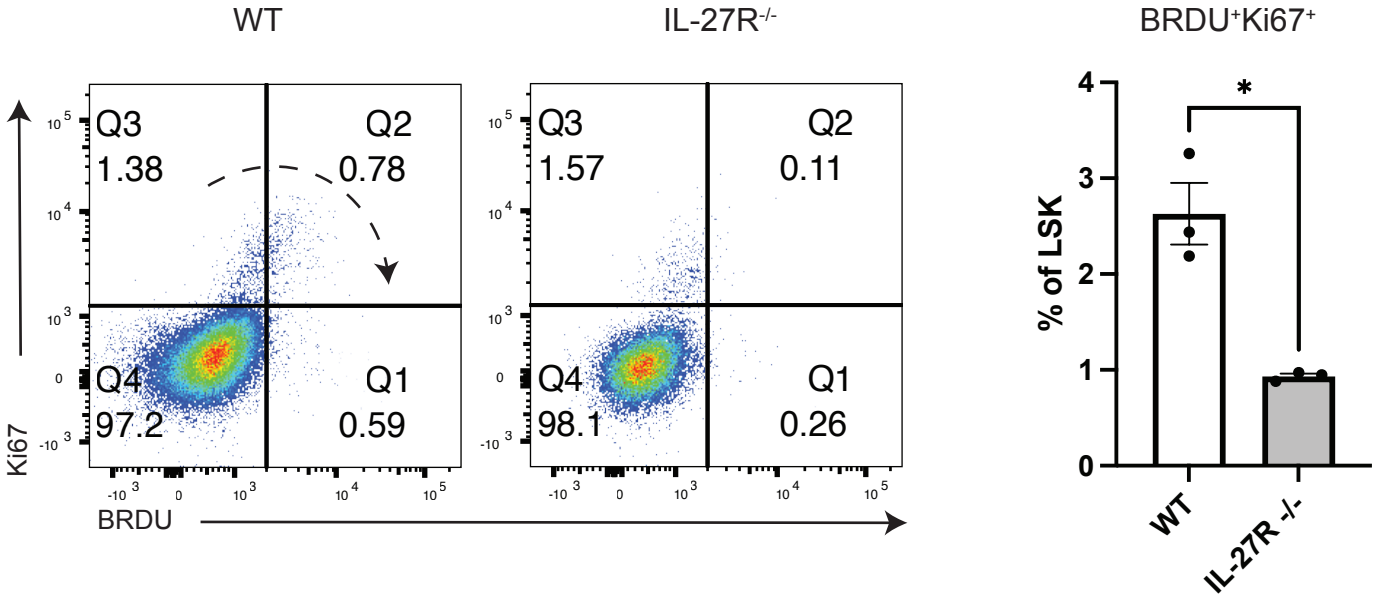

B.

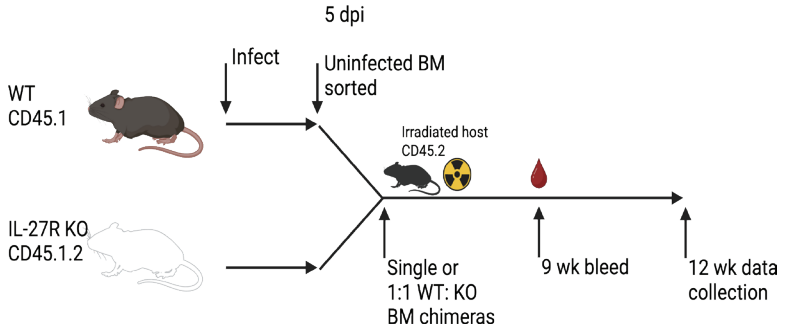

C.

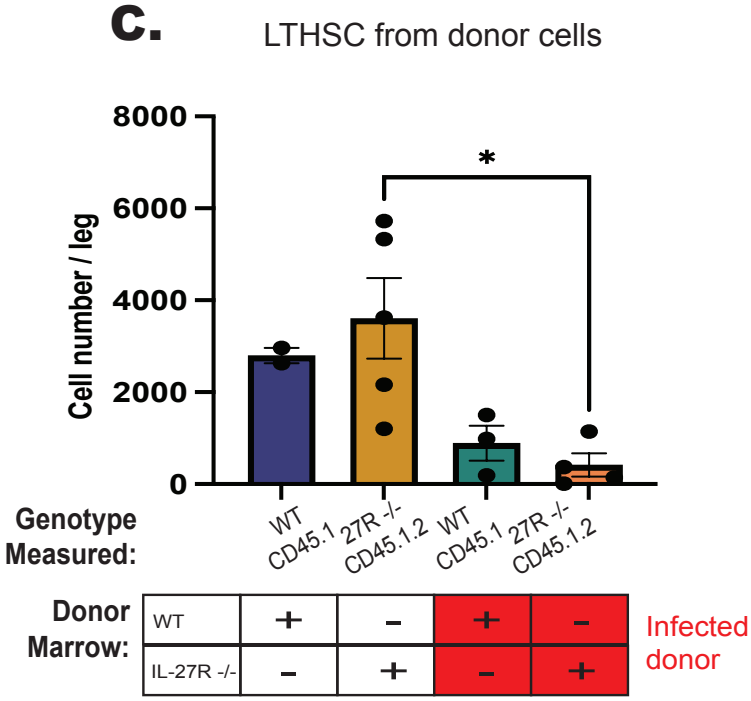

D.

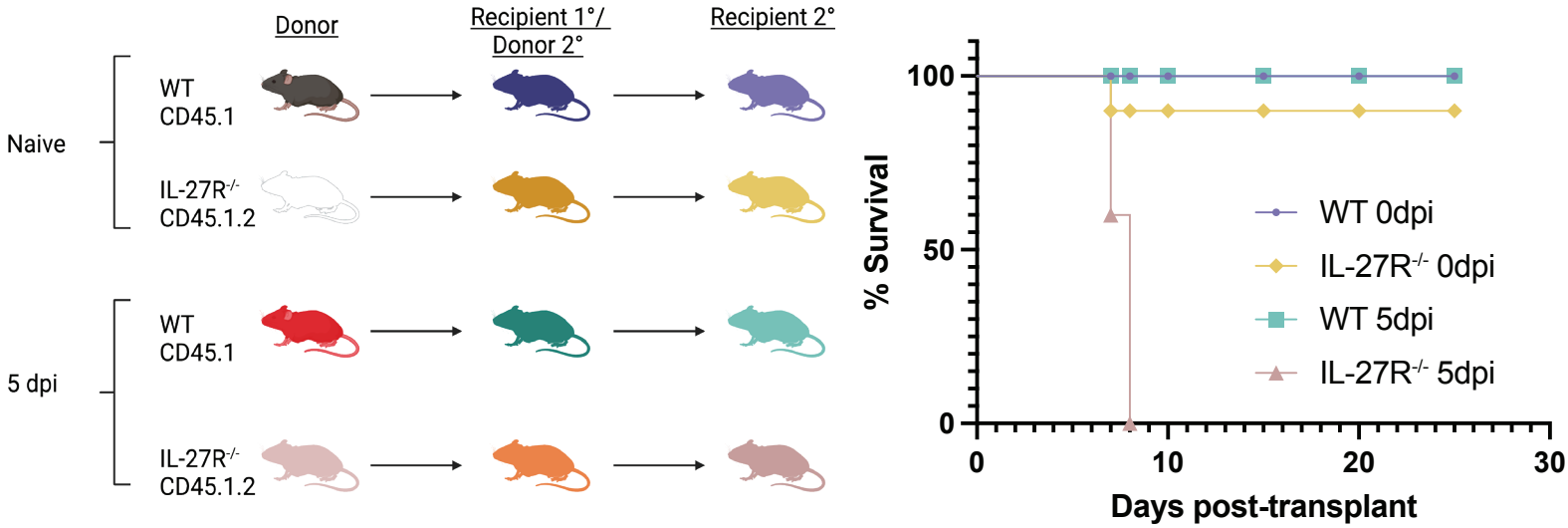

Supplemental Figure 9

A.

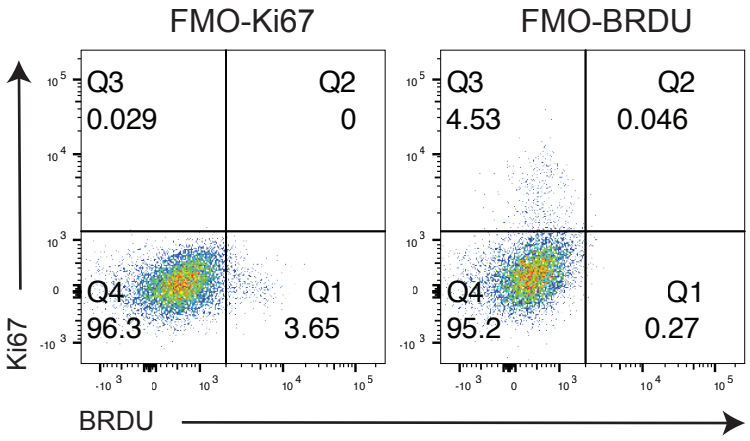

B.

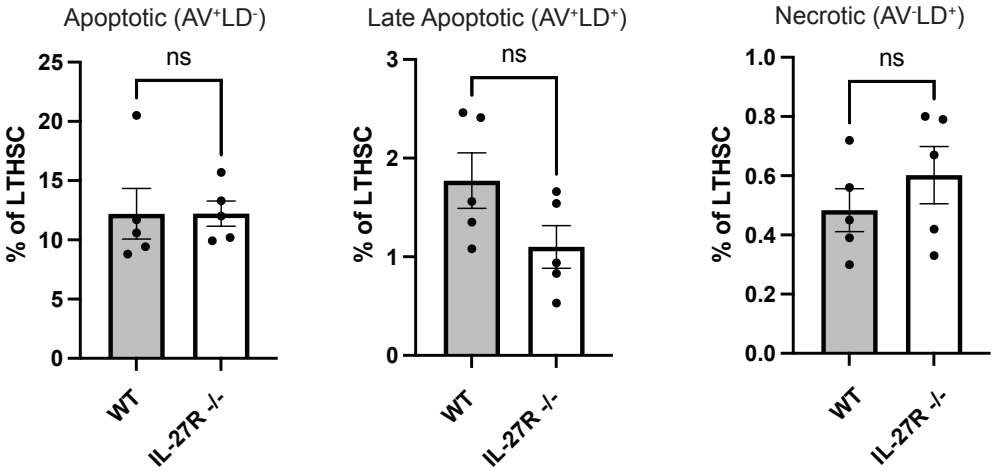
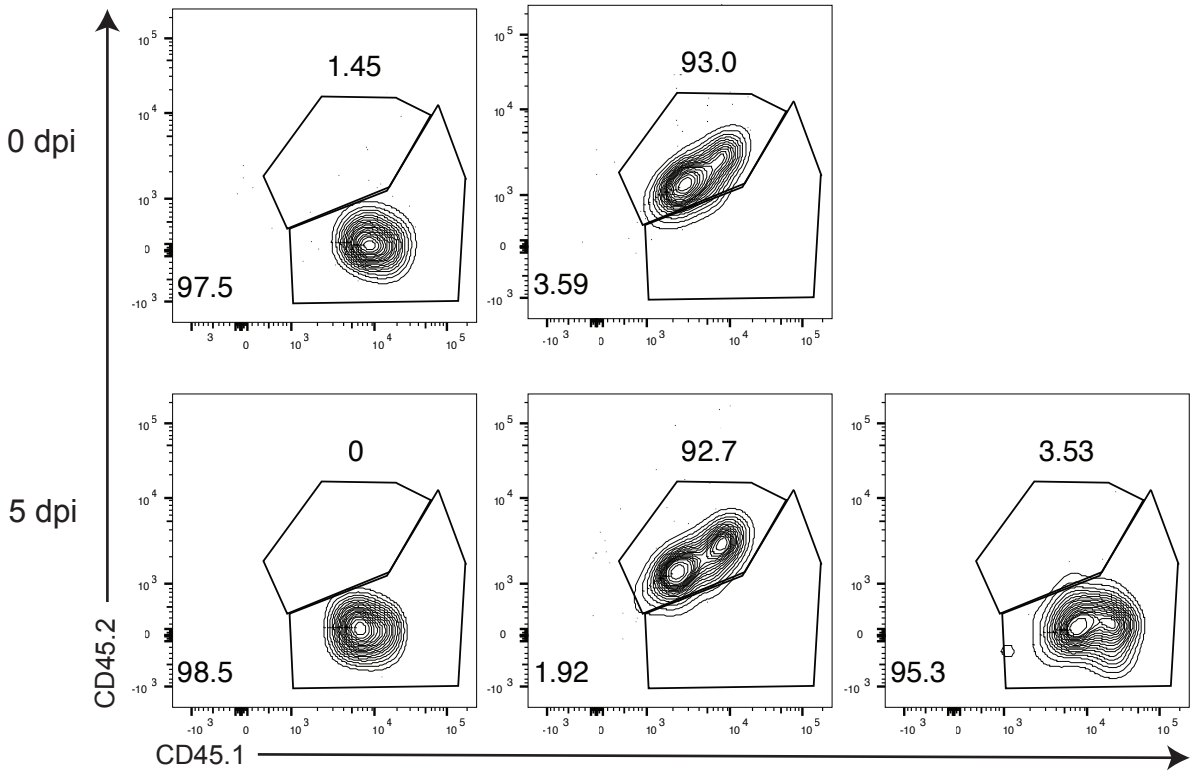
C. Donor marrow: WT IL-27R$^{-/-}$ 1:1